REPORT DOCUMENTATION PAGE

Form Approved
OMB No. 0704-0188

1. REPORT DATE *(DD-MM-YYYY)*	2. REPORT TYPE	3. DATES COVERED *(From - To)*
05/13/2010	Performance/Technical Report	Feb 2008 - May 2010

4. TITLE AND SUBTITLE
A Fluid Helmet Liner for Protection Against Blast Induced Traumatic Brain Injury

5a. CONTRACT NUMBER

5b. GRANT NUMBER
N00014-08-1-0261

5c. PROGRAM ELEMENT NUMBER

6. AUTHOR(S)
Young, Laurence, R.
Son, Steven, F.
Christou, George, A.
Alley, Matthew, D.
Goel, Rahul
Vechart, Andrew, P.
Schimizze, Benjamin, R.

5d. PROJECT NUMBER

5e. TASK NUMBER

5f. WORK UNIT NUMBER

7. PERFORMING ORGANIZATION NAME(S) AND ADDRESS(ES)
Massachusetts Institute of Technology
77 Massachusetts Avenue
Cambridge, MA 02139

8. PERFORMING ORGANIZATION REPORT NUMBER

9. SPONSORING/MONITORING AGENCY NAME(S) AND ADDRESS(ES)
Office of Naval Research
875 North Randolph Street
Arlington, VA 22203-1995

10. SPONSOR/MONITOR'S ACRONYM(S)
ONR

11. SPONSOR/MONITOR'S REPORT NUMBER(S)

12. DISTRIBUTION/AVAILABILITY STATEMENT
Approved for Public Release; distribution is Unlimited

13. SUPPLEMENTARY NOTES

20100519237

14. ABSTRACT
Development of a new ACH liner design using the novel idea of including filler materials inside channels in the liner is well underway. An energy absorbing foam has been selected for the main liner structure, and several filler material candidates of widely varying properties are being considered. To date material has been evaluated both experimentally and numerically. In the very near future tests will commence on three dimensional prototypes of the newly designed liner. Numerical studies will include coupled simulations with a detailed finite element head model, providing insight into the effect of the new liner on the brain's response to a blast wave impact.

15. SUBJECT TERMS
Traumatic Brain Injury, IED, Blast Mitigation, Blast Loading Simulation

16. SECURITY CLASSIFICATION OF:			17. LIMITATION OF ABSTRACT	18. NUMBER OF PAGES	19a. NAME OF RESPONSIBLE PERSON
a. REPORT	b. ABSTRACT	c. THIS PAGE			Andrew P. Vechart
					19b. TELEPHONE NUMBER *(Include area code)*
U	U	U	SAR	50	617-324-0529

A Fluid Helmet Liner for Protection against Blast Induced Traumatic Brain Injury

Performance/Technical Report May 2010

ONR Award Number N00014-08-1-0261

Laurence R. Young
Steven F. Son
George A. Christou
Matthew D. Alley
Rahul Goel
Andrew P. Vechart
Benjamin R. Schimizze

Table of Contents

Abstract

Development of a new Advanced Combat Helmet liner design using the novel idea of including filler materials inside channels in the liner is well underway. An energy absorbing foam has been selected for the main liner structure, and several filler material candidates of widely varying properties are being considered. To date material has been evaluated both experimentally and numerically. In the very near future tests will commence on three dimensional prototypes of the newly designed liner. Numerical studies will include coupled simulations with a detailed finite element head model, providing insight into the effect of the new liner on the brain's response to a blast wave impact.

Final Summary

The objectives of this project have been identified as the following.

1) Identify an optimal material or combination of materials to use as filler inside channels in the foam liner. The materials will be optimal in the sense of maximizing the performance characteristics of the helmet liner when subjected to a blast wave. Performance is measured by blast peak overpressure reduction, shifting of the frequency content of a blast wave to lower frequencies, increase of the peak overpressure rise time, increase of the impact duration, and reduction of the impulse transmitted through the helmet.

2) Develop and validate a computational model of the newly designed liner. The model will couple with a skull and brain model developed by Prof. Raul Radovitzky's group at MIT.

3) Construct and optimize a prototype of a functional helmet liner. Factors to be optimized include overall liner dimensions, channel geometry, and filler placement subject to the criteria listed in Objective 2.

To design and test the liner, experimental and computational techniques are used. To isolate effects of material properties on the transmitted blast wave characteristics, experiments first are carried out on "flat plate" samples. Essentially this amounts to a rectangular sandwich consisting of layers of foam, filler material, and foam, respectively. Filler materials being considered include Aerogel, Glycerin, Water, Glass Beads, and Volcanic Tuff.

For experimental work, it was necessary to ensure testing would be performed at proper blast levels for traumatic brain injuries to occur. Based on data from Kinney and Graham (1985), blast peak overpressure levels under 100 psig are sufficiently likely not to be lethal to use in these tests. Using the shock tube facility at Purdue University, the following blast profiles were obtained at various distances from the shock tube.

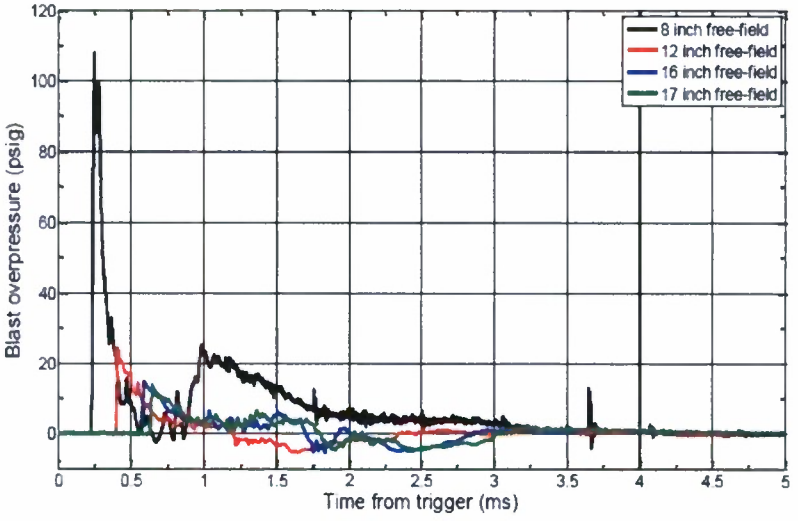

Figure 1A - Standard Experimental Loading Conditions

From Figure 1A, it is apparent that the setup at Purdue is sufficient to provide the type of blast loadings necessary for this work, particularly for loading distances of greater than 8".

Using the first iteration of the experimental set-up at Purdue, the following blast response characteristics were obtained for various filler materials.

Sample	Impulse [psig-ms]	Arrival Time [ms]	Duration [ms]	Rise Time [ms]	Peak [psig]
Free-Field	5.19	0.57	1.13	0.02	15
Solid	0.36	0.74	1.27	0.10	0.86
Cabosil	0.47	1.00	0.98	0.40	0.98
Aerogel	0.41	0.81	1.14	0.55	0.91
Expanding Foam	0.45	0.80	1.42	0.82	0.80
Tuff	0.34	1.26	1.31	0.57	0.56
Glass Shot	0.28	0.76	1.68	0.43	0.47
Water	0.38	0.83	1.53	0.60	0.57
Glycerin	0.34	0.86	1.58	0.43	0.45

Table 1A - Attenuated blast profile parameter comparison

Indications from this initial work are that Glycerin and Glass Shot (also referred to as Glass beads) as filler materials perform the best, with Volcanic Tuff and Water in a close second. In fact, the transmitted pressure using Glass Shot and Glycerin was just over half that of the Solid material, illustrating the effectiveness of including filler materials inside the foam. It should be noted, however, that peak transmitted pressure levels are very low. This posed difficulties for analysis. Therefore, a new set-up was designed. Results for testing with the new set-up are provided below.

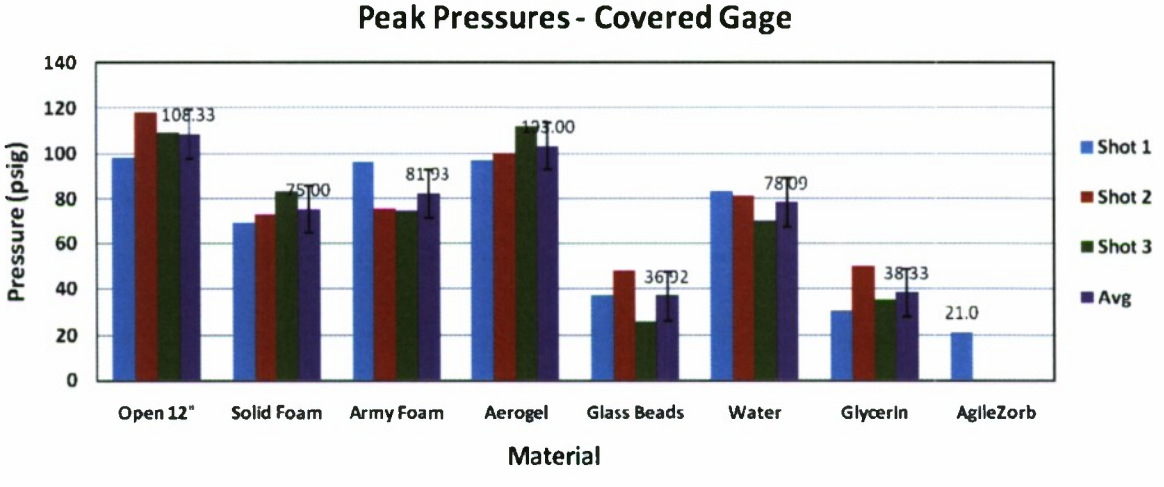

Figure 2A - Peak pressures with different filler materials using new experimental setup

The results here include testing of a material not considered for the first round of tests: AgileZorb™. The results indicate some similar results to previous results. Glass Beads and Glycerin have peak

transmitted pressures approximately half as large as those from the Solid foam cases, supporting the conclusion that inclusion of the filler materials enhances the performance of the liner.

The software ABAQUS™ is being used for numerical analysis. The main requisite for use of this software was proving it could accurately model the blast loading considered in this project. Simulations were carried out with two different loading conditions similar to those considered here. Comparison of numerically obtained results with theoretical results are provided below.

Loading	0.17 MPa			1.00 MPa		
	Theoretical	Numerical	% Error	Theoretical	Numerical	% Error
Shock Velocity, U_s [m/s]	537.82	531.72	-1.13	1055.7	1102.29	4.41
Particle Velocity, u_p [m/s]	265.62	267.9	0.85	786.75	840.5	6.81
Density Ratio, ρ_2/ρ_1	1.98	1.99	0.51	3.93	4.00	1.78

Table 2A - Numerical and theoretical values of shock wave propagation parameters for incoming wave

The results shown in Table 2A confirm that ABAQUS™ is capable of modeling a blast loading condition as required by this project.

A numerical model of the original experimental set-up has been developed. While it is still being adjusted, some results have been obtained from it to compare with experimental results.

Material	Expt/ Num	Peak Pressure (Psig)	Percentage Change (%)	Rise Time (ms)	Duration (ms)
Solid Foam	E	**0.79**	n/a	0.12	1.27
Solid Foam	N	**0.63**	-20.25	0.20	0.87
Aerogel	E	**0.81**	+2.5	0.30	0.94
Aerogel	N	**0.78**	+23.8	0.18	0.73
Glass Beads	E	**0.36**	-54.43	0.43	1.68
Glass Beads	N	**0.26**	-58.73	0.25	0.84
Tuff	E	**0.43**	-45.56	0.34	1.20
Tuff	N	**0.46**	-26.98	0.24	0.48

Table 3A - Comparison of experimental and numerical results

Some general trends can be seen in Table 3A. Glass Beads perform well, as indicated in all previous results. Of course, there is discrepancy between the experimentally and numerically obtained quantities for Glass beads and for each filler material in general. One factor contributing to the discrepancy is the variability in packing density for the experimental work. It is difficult at this point to compare the experimental packing density with that used in the numerical simulation. In the near future, characterization of a more accurate material model for the granular materials listed here will be done to improve numerical studies.

For numerical studies on the 3D liner, the liner model is in the process of being coupled with a detailed human head model from Prof. Radovitzky (Fig. 3A).

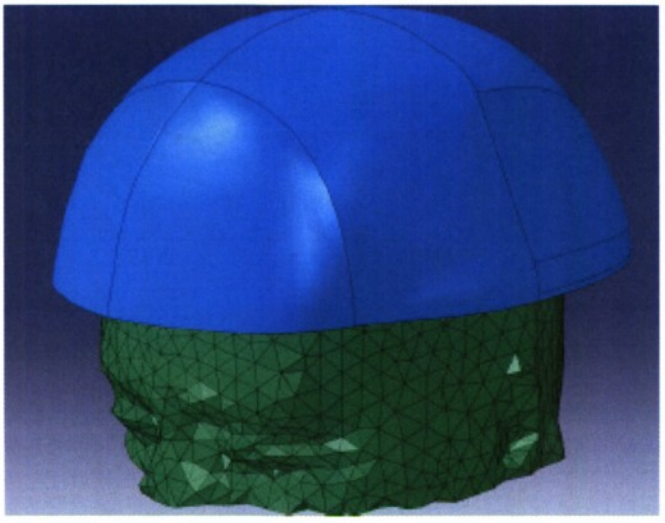

Figure 3A - Integrated 3D liner model with human head model

As of yet, definitive conclusions cannot be made. Indications so far are that including filler materials inside the liner substantially improves its performance against blast wave loading. Particularly, Glass beads and Glycerin look to be some of the most promising candidates for an optimal filler material. In the near future, a more solid conclusion regarding the best filler material will be made, and testing and simulations will begin on the full 3D liner designs.

Objectives of the Project

The ultimate goal of the project is to increase the threshold for blast induced brain injuries in response to the growing threat from IEDs in overseas conflicts. The aim of this project is to develop a new helmet liner design capable of mitigating the harmful effects of blast waves. To do so, the following objectives have been identified.

1) Identify an optimal material or combination of materials to use as filler inside channels in the foam liner. The materials will be optimal in the sense of maximizing the performance characteristics of the helmet liner when subjected to a blast wave. Performance is measured by blast peak overpressure reduction, shifting of the frequency content of a blast wave to lower frequencies, increase of the peak overpressure rise time, and reduction of the impulse transmitted through the helmet.

2) Develop and validate a computational model of the newly designed liner. The model will couple with a skull and brain model developed by Prof. Raul Radovitzky's group at MIT.

3) Construct and optimize a prototype of a functional helmet liner. Factors to be optimized include overall liner dimensions, channel geometry, and filler placement subject to the criteria listed in Objective 2.

Comparison of Actual Activities with Initially Planned Activities

-Material Research and Selection

VN 600 foam from DERTEX Corporation has been chosen for the main structure of the liner based on its ability to absorb energy as evidenced by drop-test results.

The initial list of proposed filler material configurations focused mainly on fluids having different properties. After a literature survey of blast mitigation studies, the list was modified to accommodate a wider variety of materials. Fillers considered include Air, Water, Glycerin, Aerogel, Glass shot, Microspheres, Cab-o-Sil, and Volcanic Tuff. Choice of these fillers allows for evaluation of the effect of such properties as viscosity, density, porosity, bulk modulus, particle size, and acoustic impedance on blast attenuation. Modification of the list of possible filler materials has enhanced the relevancy of the project because a more comprehensive study spanning known blast mitigation strategies now takes place. The impact of this change on the schedule of the project has been minimal.

-Material Evaluation

The original plan for material testing was to begin with low-energy tests at MIT to characterize material acoustic attenuation properties and progress to high-energy blast tests at Purdue University. This schedule was accelerated by directly starting with high-energy blast tests. Material response to blast loading can vary widely from its response to simple sonic acoustic loading, and it was decided the low-energy tests were an unnecessary extra step.

Evaluation of the material blast loading properties is being completed from two standpoints: numerically and experimentally. As per the initial plan for testing, flat-plate samples are first being tested. Experimentally, testing of this simple geometry has gone through a few iterations to improve measurement quality. This has been proceeding as originally planned.

The initial plan for numerical studies was to use a software package developed by Prof. Radovitzky and the MIT-VA team especially designed for blast loading simulations. At the beginning of the numerical studies, however, it was decided to use the commercially available finite element software ABAQUS™ instead. Its extensive documentation and general applicability to numerical simulations makes ABAQUS™ an easier software package to learn and use. The intention of using ABAQUS™, therefore, was to speed up the process of the "simple" flat plate simulations and promote continuity between researchers using the model. Because ABAQUS™ is not tailored specifically to air blast loading simulations, effort has gone into verifying that the software can, indeed, model a blast wave. Using ABAQUS™ makes it relatively easy to modify loading conditions and part geometries and easy to extract quantities of interest from simulations. There are issues still being resolved with the simulations, though once resolved the computational model should be accurate and useful.

-Development, Prototyping, and Testing of a 3D Helmet Liner

Work on the full 3D liner is proceeding as initially envisioned. The bulk of material evaluation and selection is being completed using the flat plate samples. An initial design for a liner has been built.

Originally the plan was to have micro machined channels in the foam. With the foam used here, such an operation would be very difficult (the foam is soft and deformable and has the tendency to melt) and time consuming. Prototypes are currently being constructed by attaching strips and sheets of foam in such a way to create channels. The foam parts are secured together using a high-strength adhesive spray that is chemically compatible with the foam. An experimental set-up has been prepared at Purdue University and is used for testing.

Numerically, a model of the solid liner has been developed in ABAQUS™. Channels can be included in this model however desired for parametric studies. This model is in the process of being coupled with a detailed model of the human head from Prof. Radovitzky's group. With the exception of use of ABAQUS™, activities for this part of the project have not deviated appreciably from the initial plan.

Experiments

Literature Survey

The project started with a literature survey on use of channels in helmet liners. An extensive search of journals and conference articles as well as patents was conducted. The concept of incorporating channels in sports helmet was first suggested four decades earlier. Morgan (1971) proposed a plurality of inter-connected expandable first chambers with valves placed inside the helmets. These chambers would be filled with non-compressible fluid. Upon impact, the fluid will get displaced from the first chambers to the empty second chambers and, due to the design of the chambers, the displaced fluid is returned back to first chambers after the impact force is removed. In last four decades there have been many attempts (Holt, 1972; Villary, 1976; Gooding, 1983; Hosaka, 1992; Calonge, 1998, Mendoza, 2001) in employing air bladders or fluid chambers; however, none of the proposed concepts materialized into a marketable product. Although potentially of value, none of these approaches are directly applicable to the blast protection problem. One patent that discusses blast protection is by Ponomarev (2006). It describes a method for placing a partially evacuated chamber filled with air or another gas between the blast source and the object to be protected, including the body. The chamber ruptures under the incoming pressure peak and the relative vacuum "sucks up" the ambient air, creating a negative pressure wave to interfere with the positive wave from the blast and reduce the transmitted pressure. Stuhmiller (2008) suggested a cushion for use in body armor to mitigate shock loads. It may include a plurality of fluid pockets which could be deformable or reconfigurable, and are therefore connected to empty reservoir pockets. Transport of fluid was suggested through a vent controlled by a valve.

There has been limited research on use of filler materials in body armors. Gerber (1987) and Groves (1992) suggested use of compressible materials in the form of glass beads for use in body armor. Rhoades (2004) suggested use of a shear thickening material made of Polyborosiloxane for sports padding, bulletproof vests, weaponry etc.

An extensive literature survey was also conducted on material properties which are hypothesized to provide blast attenuation. Mechanical properties contribute largely to the behavior of shock wave interactions at material interfaces. Depending on the acoustic impedance of the interacting medium, the shock wave will reflect, transmit, and dissipate to differing degrees. A representative study presented by Zhuang et al. (2003) examined scattering effects of stress waves in layered composite materials. It was determined that the large impedance mismatches imposed at the interfaces created larger rise times for the shock front, essentially lengthening the time for a maximum stress to be obtained under a given loading condition. Advancing the idea of internal interfaces providing dissipation and dispersion effects, the representative computational study by Li et al. (2002) examines the effect of a multitude of interfaces by means of cellular media. Cellular collapse at low velocity impacts was verified to attenuate energy transfer effects. However, in the area of high velocity (blast) effects, it has been suspected that the cellular media actually enhanced the effect severity. Allen et al. (2003) presents suggestions for the mechanisms of blast mitigation including porosity, inertial effects (density), and thermal dissipation (liquids). The presence of liquid can allow explosive energy to be transferred to kinetic energy. Presence of pores can help in attenuation by dispersion at 3D porous surfaces. Nesterenko et al. (2003),

suggested use of granular material, proposing that it would be able to scatter the wave as well as absorb energy due to compression. Homae et al. (2007) suggested use of water/mist, proposing that phase transition could probably provide attenuation. In our previous studies here at MIT, for impact tests, Stewart (2008) had shown the effectiveness of Glycerin as a possible way to reduce the transferred impact forces by viscous dissipation and compression of foam.

In order to test each of these proposed mechanisms, experiments were established to measure free field air blast parameters from an unconfined, unobstructed explosive charge. Subsequent experiments were then performed with the explosive charge confined in the various mitigant materials.

The thermal and viscous effects were examined using Glycerin and Water which provided different heat capacities. The porosity and density effects were examined using Aerogel, Glass Beads and Volcanic Tuff. The results of the experiments suggested that thermal effects were insignificant, at least in relation to inertial and porosity effects. The final key findings of the experimental results suggested that a higher density material provided better mitigation, and similarly for higher viscosity.

A previous study supports an estimate of 1% probability of fatality at 100 psig and 90% probability of fatality at 220 psig (Kinney and Graham, 1985). Therefore, it was determined that levels below 100 psig would be sufficient for laboratory testing to characterize system response to a loading condition in the field producing injury but not necessarily fatal injury.

Methods

After specifying the overpressure range of interest, necessary standoff distances were determined. As the focus of this study was presented to be small-scale laboratory testing methods for TBI occurrences, small 3 gram charges of Pentaerythritol Tetranitrate (PETN) plastic sheet explosive were used in the experiments providing an explosive yield of 13.24 kJ and having TNT equivalent mass of 2.87 grams. The PETN plastic sheet explosive consisted of 63% PETN powder, 29% plasticizer, and 8% nitrocellulose with a density of 1.48 g/cm^3 and detonation velocity of 6.8 km/s. Initiation of the PETN was produced by a chain of 50 grain detonation cord.

The interaction of the blast wave was introduced by means of a uniquely designed explosive-driven shock tube (Fig. 1) intended to direct the blast energy toward the target. The shock tube design consisted of a 12 in. detonator chamber capped at one end and a 36 in. HE chamber also capped at one end. The detonator chamber prevented fragmentation from the aluminum detonator cap into the room and target as the focus of these studies was on the blast itself and not fragmentation of any kind. The long HE chamber provided extra distance for shock wave/product separation as well as minimized reflections and turbulence at the exit. Shock waves fundamentally occur only in supersonic conditions whereas the combustion products travel approximately at local sonic speeds. Therefore, the additional length of the HE chamber provided greater separation for imaging purposes as well as spatial distribution to smooth the blast wave compared to the blasts of open air charges closer to the targets.

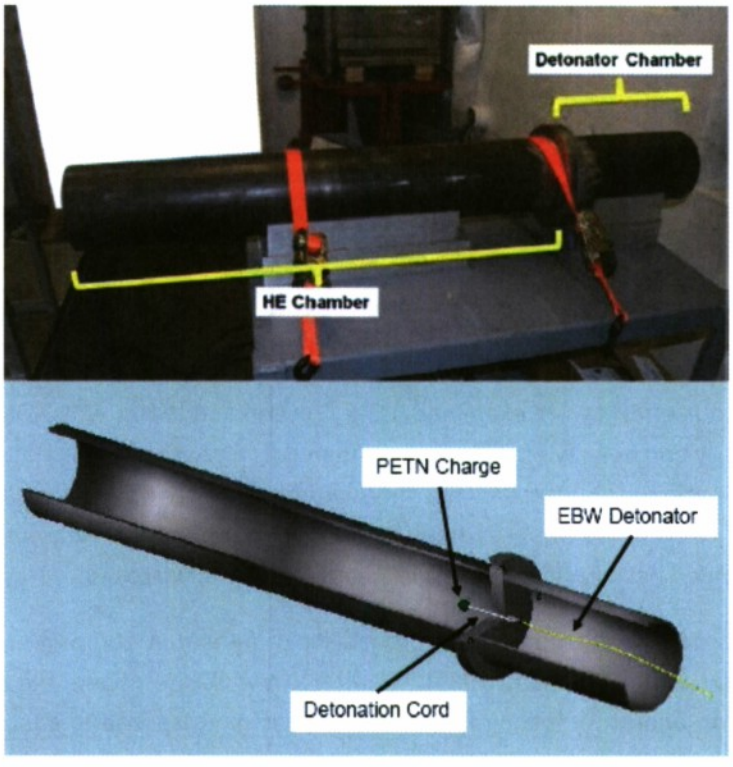

Fig. 1 Explosive driven shock tube

In reference to imaging, high-speed shadowgraph imaging was performed for visualization of the experimental blast waves. The shadowgraph imaging provided a qualitative representation of the shock wave interaction with the various models being studied as well as quantitative data regarding the shock wave parameters. Fig. 2 shows schematics of the shadowgraph setup.

The blasts were measured using PCB model 137A24 free field blast pressure pencil probes. The gauge measurements then were conditioned and amplified using PCB model 482A22 signal

Conditioners and the data were recorded using Tektronix DPO4034 oscilloscopes.

Table 1 and Fig. 3 provide the actual measured blast parameters of the standard loading conditions and the representative plots. Finally, in order to validate the blast measurements being made, 12 experiments performed without targets at 12" distance to compare the repeatability of the small-scale blasts. The results of the 12 experiments resulted in standard deviations of 10% for impulse, less than 5% for arrival time and duration, and 15% for peak overpressure suggesting acceptable overall repeatability in the method.

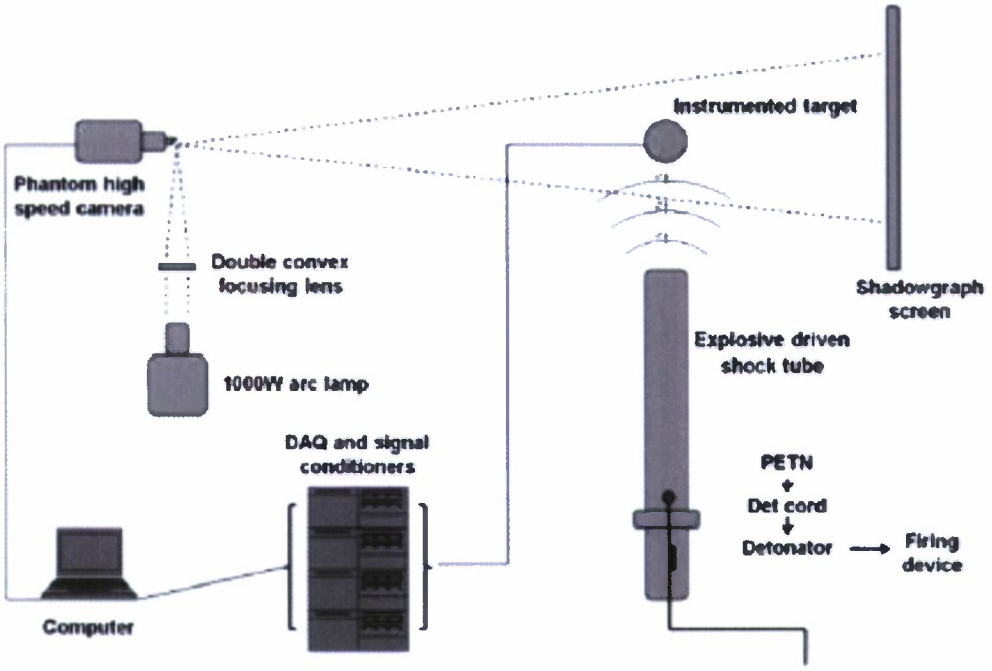

Fig. 2 Sketch of experimental setup, Shadowgraph Method

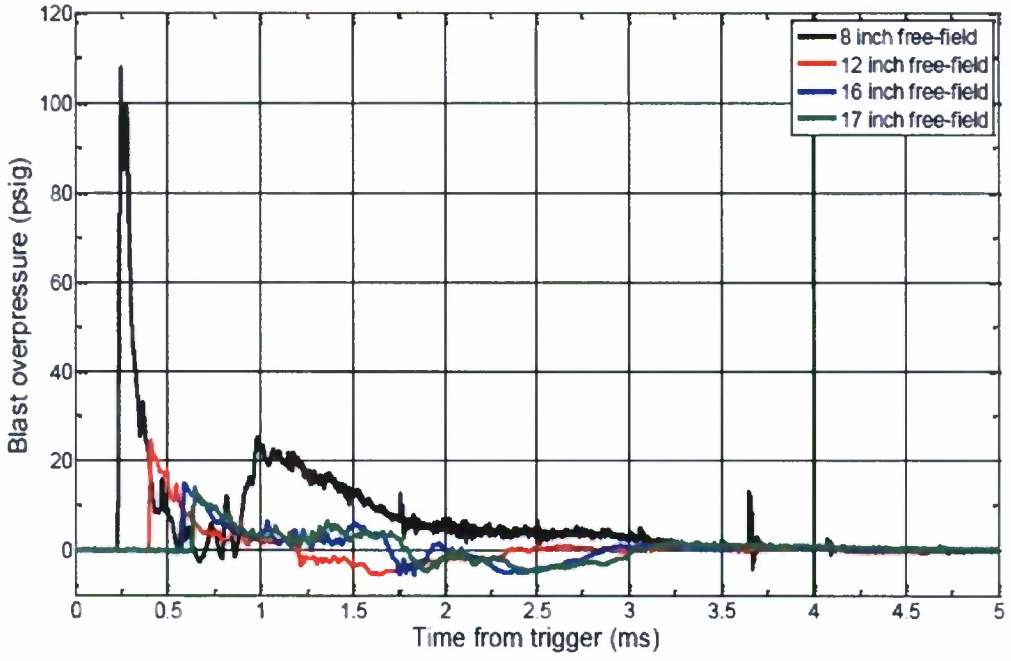

Fig. 3 Standard experimental loading conditions

Table 1. Measured parameters for standard loading conditions.

Standoff	Impulse [psig-ms]	Positive Arrival [ms]	Negative Arrival [ms]	Duration [ms]	Peak [psig]
8 inch	10.68	0.21	0.64	0.43	108.10
12 inch	5.00	0.39	1.21	0.81	24.82
16 inch	5.19	0.57	1.71	1.13	15.01
17 inch	5.18	0.63	1.80	1.17	13.98

Filler Materials

In order to fulfill the stated objectives of the blast mitigation work, it was necessary to study the effects of various materials obstructing the flow of a blast wave and the ability of the given material to reduce the damage caused by the blast. The general theory being applied to this research is that the greatest energy transfer within the obstructing material will yield the greatest mitigation effects to the blast.

In order to accommodate large energy transfers resulting in significant blast attenuation, composite structure material samples were fabricated. A common material was defined as the control material in which filler materials would be added. This control material was vinyl-nitrile VN-600 foam from DERTEX Corporation. The foam is characterized by the company as a microcellular, energy-absorbent foam with a density of 108 kg/m^3. This specific foam was selected because of its good energy absorbing characteristics that were determined during drop test experiments on flat foam samples as compared to other conventional foam types such as Expanded Polystyrene (EPS) and Polyurethane (PU) (Stewart, 2008). There was a significant reduction in measured peak accelerations and forces on head forms that were dropped on VN 600 foam compared to EPS and PU helmet liners. The control sample was a solid foam sample of size 10 in. x 10 in. x 1 in. with a total volume of 100 in^3. The samples following the control consisted of the same outer control foam with a single-cavity removed core. The cavity for each sample was of size 8 in. x 10 in. x 0.5 in. for a total volume of 40 in^3. The cavity was then filled with varying materials as shown in Table 2 and sealed to prevent escape upon loading. Fig. 4 shows the test samples.

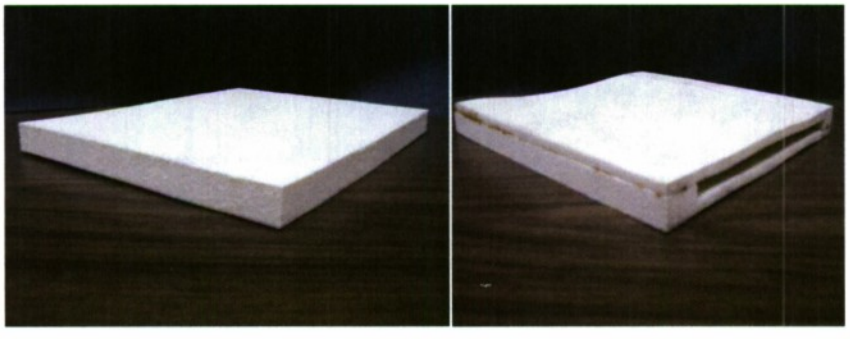

Fig. 4 Test samples. (Left) Solid Foam Control Case, (Right) Single Cavity Sample

The filler materials that were introduced were intended to span a range of possible attenuating features. The main material characteristics that have initially been studied with this work were viscosity, density (and therefore impedance and sound speed), and particle size. The effects of viscosity were studied by comparing the attenuating features of water filled foam samples and glycerin filled foam samples. The variation in viscosity between the two liquids is three orders of magnitude as water has a viscosity of approximately 9E-4 Pa-s while glycerin has a viscosity of approximately 1 Pa-s. In addition to viscous effects, the liquids also varied in density, therefore affecting sound speed and acoustic impedance. Particle size was varied between three powders: Aerogel, Cabosil, and Glass beads. The difference in particle size could allow for variation in packing density and particle contact. Increased particle contact might suggest better wave transmission as the wave would be passing through interfaces with matching impedances. Density was essentially varied between every material. Aerogel and Cabosil provided low range densities; Water, Glycerin, and an Expanding spray foam provided midrange densities; and the Glass beads and Volcanic Tuff rock provided high-range densities. As stated previously, the density variations directly affected material sound speed and acoustic impedance. Each of these factors then contributed to the behavior of the wave transmission. With higher impedance values, greater wave energy would potentially be reflected. With decreased sound speeds, the component of the wave that was actually transmitted would transmit slower and potentially be delivered behind the material with a less severe rise. These filler materials were tested in the single cavity sample, placed at 12" from shock tube. At this distance the peak overpressure experienced was 25 psig, which can cause mild TBI.

Table 2 shows for the properties of the filler materials

Table 2. Filler material properties

Filler	ρ (kg/m^3)	Particle size (μm)	C_0 (m/s)	Z (x10^3 kg/m^2-s)
Water	1000	n/a	1500	1500
Glycerine	1261	n/a	1900	2400
Aerogel	5-200	1000-5000	70-1300	10
Cabosil	35-60	0.2-0.3	100-1500	5-100
Expanding Foam	1060	n/a	-	-
Glass shot	2500	250-420	3700-5300	10000
Tuff (Volcanic rock)	1300	n/a	-	-

Old Experimental Setup

Initial testing was performed with the testing apparatus as described previously. However, after several experimental trials with various samples, measurement flaws were determined. By comparing shadowgraph images with datasets taken from the instrumentation, it was determined that the

measured profile was subjected to contributions from the transmitted wave as well as the initial incoming wave converging over top, bottom, and sides of the sample. Time comparisons revealed that the converging contributions of the wave traveled at much faster speeds than the transmitted wave allowing for the transmitted portion to be overtaken. Therefore, the pure transmitted wave was unreadable. In order to isolate the pure transmitted wave, a Plexiglass chamber was constructed to attach to the stand structure behind the material sample. The chamber was constructed from 0.25 in. thick Plexiglass panels 16 in. in length by 7.5 in. in width. The back end was left open to allow pressure sensor placement. Each foam sample was first sandwiched between two 10 in. x 10 in. x 0.125 in. sheets of Plexiglass to assist in sustaining structure of the sample. The back Plexiglass sheet was secured to the Plexiglass chamber by epoxy. The effective thickness of the entire composite sample structure was then 1.25 in.. Although the Plexiglass added additional layers/interfaces which would add to the attenuation effects, each sample was tested in this configuration to sustain continuity between trials. The single pressure sensor was then extended into the chamber and located at 2.75 inches behind the back face of the sample, therefore at a 16 inch overall standoff distance for easy comparison with free field standard loading profiles. The front face of the composite sample structure was still located at a 12 inch standoff distance from the mouth of the shock tube. Fig. 5 shows full view of test stand apparatus.

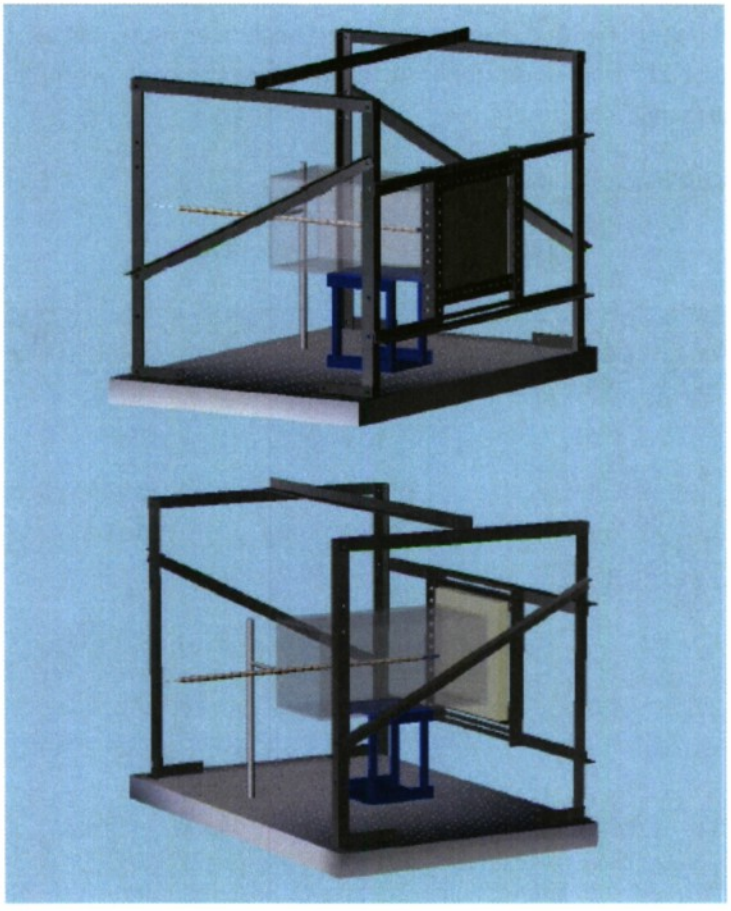

Fig. 5 Blast Mitigation Test Stand Apparatus. Front view (top) and Back view (bottom)

Results and Discussion

The final results of the mitigation experiments suggested significant attenuation characteristics for each sample. However, significant trends and distinctions were seen between groups of samples. The samples filled with Aerogel, Cabosil, and the Expanding spray foam, which are all porous materials, retained blast profiles more closely resembling air blast profiles. Specifically, negative phases were present in the transmitted waves as opposed to the remaining filler materials. Peak pressure magnitudes were close to that of the solid foam sample, therefore greater than the magnitudes measured from the remaining fillers. The transmitted wave profiles for these porous fillers also exhibited greater initial slopes from arrival time to time of peak magnitude, slowly approaching a shock front. However, the rate of rise was still less than the solid foam control sample and the free field profile. The resulting behavior similar to air blast profiles suggests the importance of the impedance mismatching characteristic. These three fillers had the lowest impedances of the fillers being studied, therefore presenting the least mismatch between air and the respective filler. This would suggest the greatest transmission of the wave and, therefore, the least attenuation.

The higher density solid materials (Glass beads and Volcanic Tuff rock) exhibited superior attenuation behavior. Both filler materials exhibited similar transmitted wave behavior with peak pressure magnitudes nearly half that of the low-range density fillers and the solid foam control sample. The Glass beads sample exhibited the longest positive pulse duration of all materials tested, with a 48% extension of duration over the free-field loading condition. The Volcanic Tuff sample exhibited more average positive pulse duration with only a 16% extension of duration. Rise times for both samples also were on an average scale. Arrival times differed slightly between the Volcanic Tuff sample and the Glass beads sample. The Volcanic Tuff sample actually exhibited the latest arrival time suggesting a significantly low density resulting in the slowest sound speed while the Glass beads sample exhibited the fastest arrival time.

The remaining two fillers, Water and Glycerin, exhibited similar trends to each other as well as the high-range density fillers. Specifically, peak pressure magnitudes were nearly half that of the solid foam control sample and the low range density samples. Durations were again lengthened compared to the air blast profile, the solid foam control sample, and the low-range density fillers. Rise times for both liquids were on the average scale while the positive pulse durations were among the highest, second only to the previous Glass beads sample. The anticipated viscous effects did not show significant behavior. Although the distinctions between the two liquids were minimal, the increased flow resistance and shear between fluid layers might suggest additional energy dissipation and wave delay superior to water as evidenced by the slightly varied measured profile.

In addition to attenuation by means of impedance mismatches, particle fracture was also suggested in the literature as a means of energy dissipation. Therefore, the foam samples with powder fillers were emptied of the filler materials following the experiments in order to collect expended filler samples. Small samples of each of the powder fillers were examined microscopically for evidence of significant fracture. It was observed that no distinguishable fracture was evident in any of the powder fillers except the highly porous Aerogel. The comparison of the Aerogel prior to the blast and following the blast

showed generally smaller particle sizes of the post-blast material (approximately 1/3 to 1/2 the original size), visible to the naked eye.

The attenuated blast profile parameters are shown together in comparison to the free field loading condition in Table 3. Additionally, sequential shadowgraph frames are shown in Fig 6 representing the passage of the blast wave external to the Plexiglass chamber and therefore successfully isolating the transmitted wave. The images show the typical incident blast wave impinging on the material sample as well as the strong reflected shock from the mitigation material. Figs. 7-9 shows blast profiles of different filler materials as compared to solid foam.

Table 3. Attenuated blast profile parameter comparison

Sample	Impulse [psig-ms]	Arrival Time [ms]	Duration [ms]	Rise Time [ms]	Peak [psig]
Free-Field	5.19	0.57	1.13	0.02	15
Solid	0.36	0.74	1.27	0.10	0.86
Cabosil	0.47	1.00	0.98	0.40	0.98
Aerogel	0.41	0.81	1.14	0.55	0.91
Expanding Foam	0.45	0.80	1.42	0.82	0.80
Tuff	0.34	1.26	1.31	0.57	0.56
Glass Shot	0.28	0.76	1.68	0.43	0.47
Water	0.38	0.83	1.53	0.60	0.57
Glycerin	0.34	0.86	1.58	0.43	0.45

Fig. 6 Shadowgraph images of Solid Foam control sample

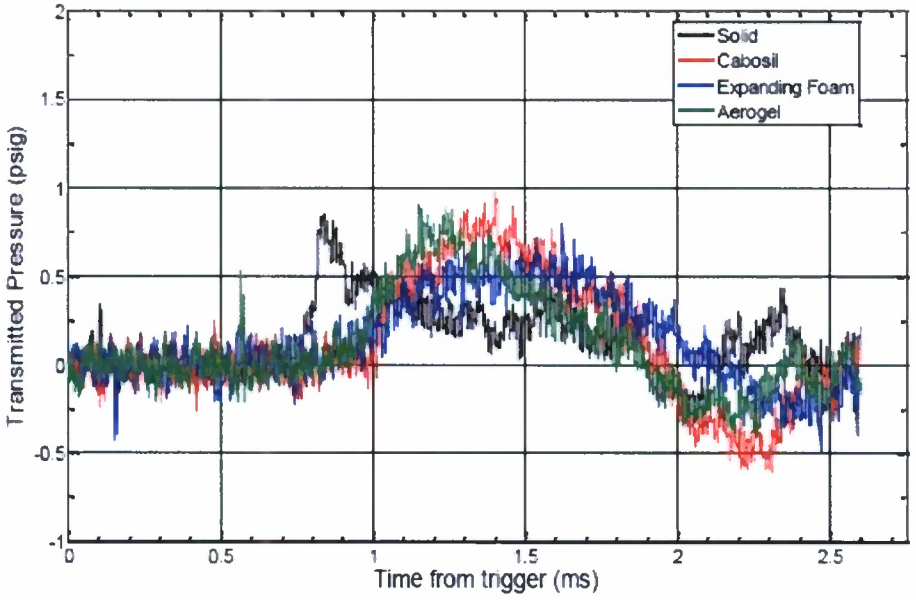

Fig. 7 Blast profiles for low density solid fillers compared to control sample

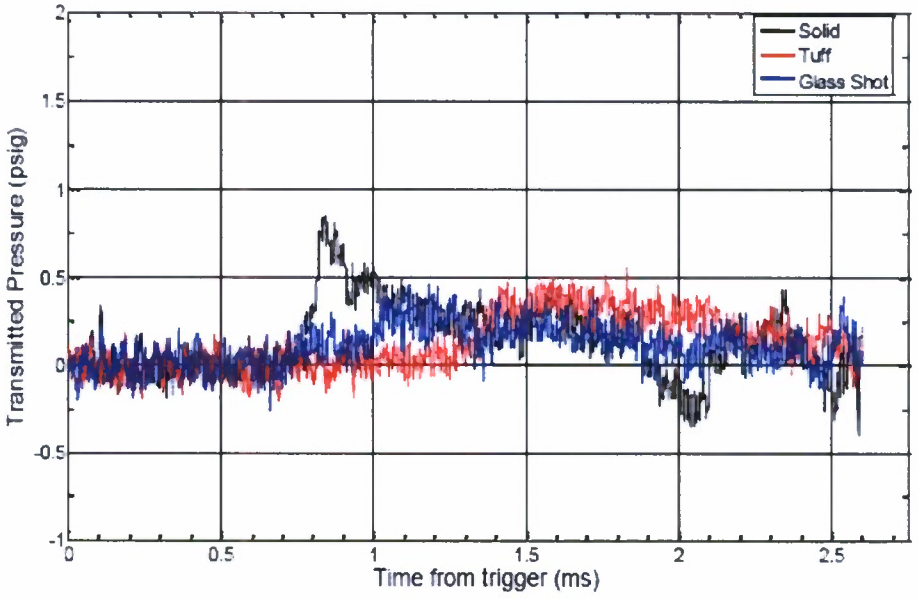

Fig. 8 Blast profiles for high density solid fillers compared to control sample

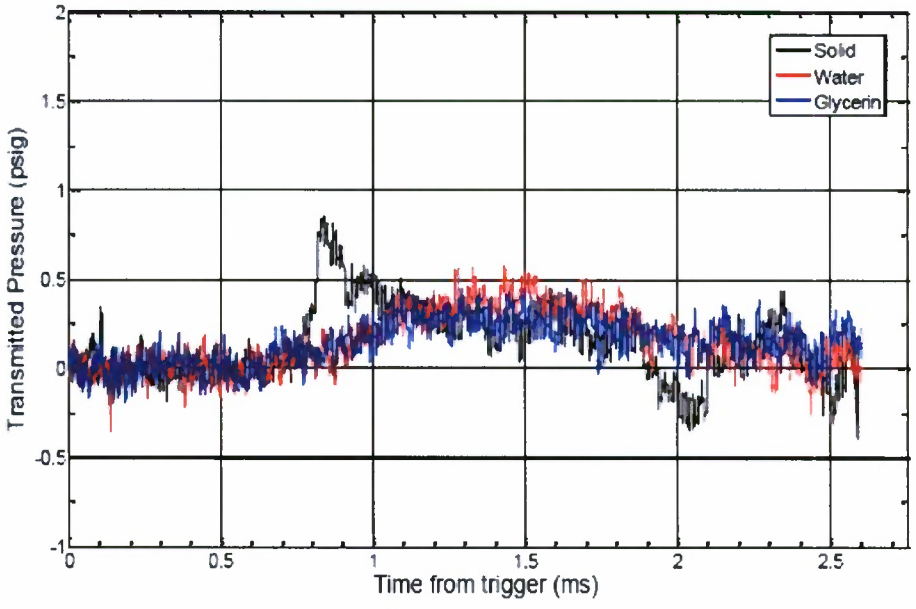

Fig. 9 Blast profiles for liquid fillers compared to control sample

Conclusions

Within the range of experiments conducted so far, the effects of particle size were non-distinguishable on the scale of the measured transmitted profiles. Although, additional energy dissipation might be enhanced through variation of particle size, those effects were not noticeable according to the calculated profile characteristics. Furthermore, viscous effects also seemed minimal. The material characteristics which resulted in the most distinguishable attenuation were porosity and density. The effect of high porosity was the retention of air blast characteristics. The higher densities contributed to larger impedance mismatches between air and the sample which results in a greater wave reflection and therefore less energy transmission through the material into a potential target. The summary of these results suggests porosity and density (impedance) dominate in the attenuation effectiveness. Air blast characteristics could be essentially eliminated with the less porous and higher density materials. Impedance mismatches dominate in that the greater variation in material property between interfaces, the less the wave will be transmitted.

New Experimental Setup

Considering low pressure levels and high noise to signal ratio as in Figs. 7-9, it was decided to change the experimental setup. Fig. 10 shows front and back views of the new experimental assembly. Essentially small samples were fixed to a steel plate as shown on the left of Fig. 10, without the need for any Plexiglass chamber. Dimensions for control sample were 5 in. x 5 in. x 1 in. as opposed to 10 in. x 10 in. x 1 in. in the previous setup. The samples following the control consisted of the same outer control foam with a single-cavity removed core. The cavity for each sample was of size 5 in. x 3 in. x 0.5 in. Two pressure measurements were recorded. One pressure gage, called covered gage (the one on the right, in

right side Fig. 10) is located exactly behind the center of the sample. It is recessed into the steel plate and kept few mm behind the back surface of the sample. The in between space is filled with thermal grease, which enhances wave transmission. Another pressure gage, called uncovered gage (the one on the left, in right side Fig. 10) is kept 3 in. laterally away from the first pressure transducer at the same height. This is located outside the periphery of the sample, and is used to record an external measurement of blast wave, which is then used to check for consistency between different shots.

Fig. 10 New experimental assembly. (Left) Front view, (Right) Back view.

Filler Materials

With this new setup, Water, Glycerin, Glass beads, Aerogel and AgileZorb™ were tested. AgileZorb™ is a patented material manufactured by AgileNano. It has essentially nano-sized pores suspended in non-wetting liquid. When the pressure exceeds a threshold, because of capillary effect, the liquid will go inside the pores, and this will dissipate energy. Once the pressure is removed, because of internal pressure of compressed air in the pores, the liquid is pushed out of pores. This way it can be reused. Due to the small size of the pores, AgileZorb™ reacts in 0.1-1 μsec, many times faster than conventional materials. This short response time is very essential for high frequency blast phenomenon.

Results and Discussion

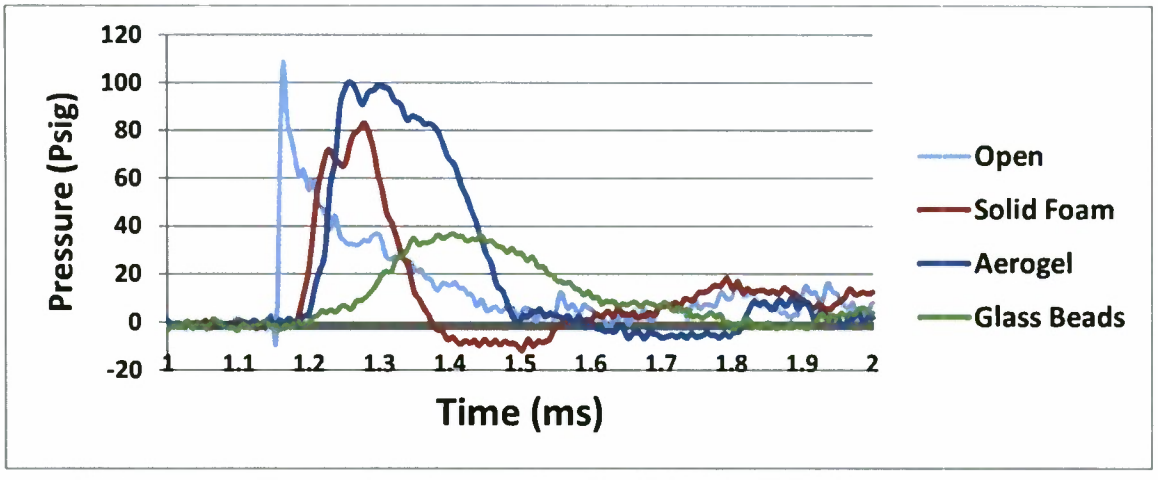

Fig. 11 Pressure profiles: Solid fillers compared to Open

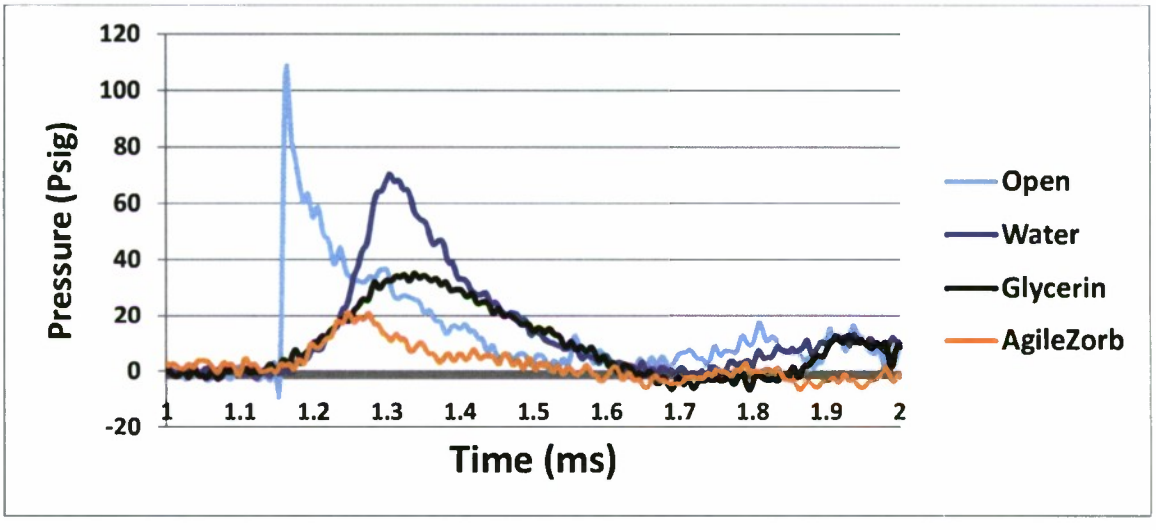

Fig. 12 Pressure profiles: Liquid fillers compared to Open

Figs. 11 and 12 shows pressure profiles for that trial of each material, which had peak pressure closest to the average. Four or five trials of each material type are conducted until three acceptable measurements are obtained. Pressure measurements for a trial are discarded if uncovered gage measurement for that trial falls outside +/- 10% of the average. In Fig. 11, it can be noted that Glass beads not only reduced the peak pressure but have also increased the time duration and rise time. In Fig. 12, Glycerin shows similar behavior as Glass beads. It is also quite encouraging to see that AgileZorb^{TM} has also substantially reduced the peak pressure. So far, we have done only one trial with this material, other trials will be carried out in few days.

Table 4 provides the peak pressure values for the three trials of each material type. It also provides the average peak pressure, the standard error and the p-values. For p-values an independent t-test is

conducted between each material type and the solid foam control case. Open 12" means that no foam sample is kept on the steel plate. Solid foam case is used as the control case. Average peak pressure for Solid foam is 75 psig. In accordance with our results with the previous setup, Aerogel, didn't provide any attenuation. In fact, it was worse than our control case. Army foam tests were conducted with the standard pads used in the Army's Advanced Combat Helmets. The difference in average peak pressure between solid foam control samples and the army foam was not statistically significant. Similarly, water did not provide any attenuation, and the difference is not statistically significant. Both Glass beads and Glycerin provided nearly 50% attenuation in peak pressure. Average peak pressure observed for Glass beads is 36.92 psig, whereas for Glycerin is 38.33 psig. The difference between the means of Glass beads and solid foam control case as well as the difference between the means of Glycerin and solid foam control case is statistically significant. Contrary to the results with the previous experimental setup, there was significant effect observed between Glycerin and Water cases, suggesting probable effect of viscosity. Interestingly, single trial results from AgileZorb™ are the most encouraging. Peak pressure observed using AgileZorb™ was only 21 psig, as compared to 75 psig of the solid foam control sample, which is essentially nearly 70% reduction. More trials of this material will be conducted to validate these results.

Fig. 13 reiterates the same results as shown in Table 4, but in bar plot form. One can again clearly see the effectiveness of Glass Beads, Glycerin and AgileZorb. The bars in Fig. 13 indicate standard error.

Table 4. Results of filler materials with new experimental setup

Material	Peak Pr - Shot 1 (psig)	Peak Pr - Shot 2 (psig)	Peak Pr - Shot 3 (psig)	Avg Peak Pr (psig)	Std Err	p-value
Open 12"	98	118	109	108.33	5.78	0.01
Solid Foam	69	73	83	75.00	4.16	-
Army Foam	96	75.3	74.5	81.93	7.04	0.5
Aerogel	97	100	112	103.00	4.58	0.02
Glass Beads	37	48	25.8	36.92	6.42	0.01
Water	83	81	70.3	78.09	3.95	0.2
Glycerin	30	50	35	38.33	6.01	0.01
AgileZorb	21	-	-	21	-	

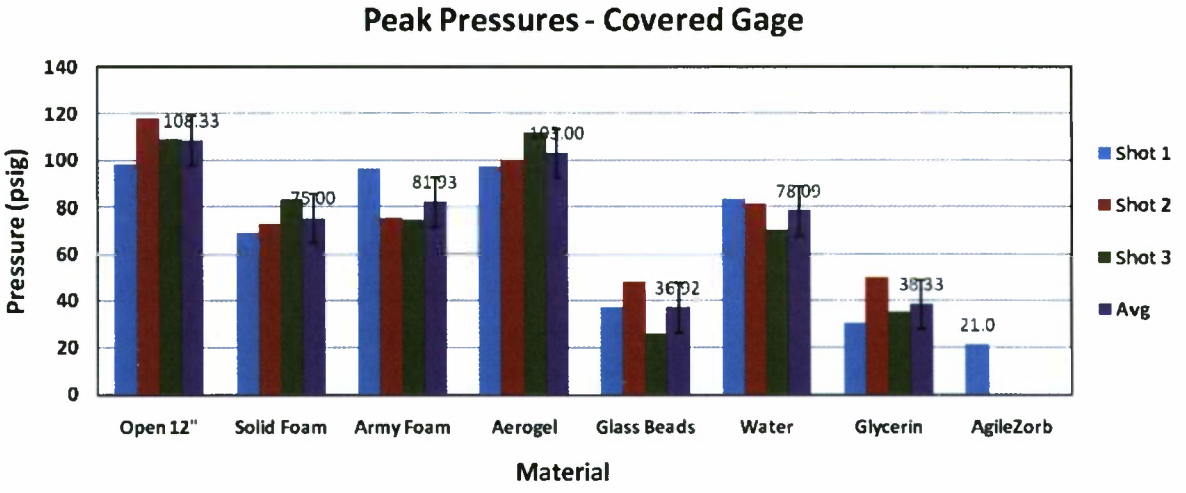

Fig. 13 Peak pressures with different filler materials using new experimental setup

Conclusions

To summarize the results using new experimental setup, it seems high density and low porosity material like Glass bead provide higher attenuation compared to low density and high porosity material like Aerogel. We also observed the increased duration and rise time for Glass beads and Glycerin, leading to reduced pressure gradients. This result is consistent with our findings using the old experimental setup. But, contrary to our findings using the old setup, viscosity does seem to have provided more attenuation compared to water. More trials need to be conducted with AgileZorb™, before any causal inference can be deduced about this material, but it does seem quite promising.

Numerical Model

The modeling of both solid and fluid domains requires the use of a coupled Eulerian–Lagrangian computational domain available in ABAQUS™ 6.9. The Lagrangian mesh is assigned to the solid geometry while the Eulerian mesh is primarily assigned to the surrounding air and to the fluid filler materials of the internal sample cavity.

In a traditional Lagrangian analysis nodes are fixed within the material, and elements deform as the material deforms. For Lagrangian elements, the material boundary coincides with an element boundary. On the other hand, in an Eulerian analysis nodes are fixed in space and material flows through elements that do not deform. Lagrangian mesh is used for solid materials (foam and solid fillers) because it helps in understanding the deformation of material as a result of blast loading. Air is modeled as Eulerian, because the pressure gage used in the previous experimental setup was located 2.75 in. behind the sample. In order to numerically measure the pressure at a specific distance from the sample, it was necessary to use Eulerian elements, as the elements do not deform as the shock wave propagates through them.

Validation of Shock Wave Propagation

To begin with, it was necessary to validate numerical shock wave propagation through air in ABAQUS™. This was accomplished by comparing the numerically derived shock velocity and density ratio across the shock with the theoretical values, from Shock-Jump relations.

For this, an Eulerian air domain of 5 m x 5 m x 200 m dimensions was created and meshed using 40 cubic Eulerian linear solid continuum elements of 5 m edge length. The application of the desired loading was uniformly applied on the top face of the Eulerian domain while the amplitude was constant for the whole duration of the simulation. The meshed computational domain employed for this study is depicted in the following Fig. 14. The figure illustrates the pressure values during a time increment in which the incoming wave has not yet reached the bottom reflective surface.

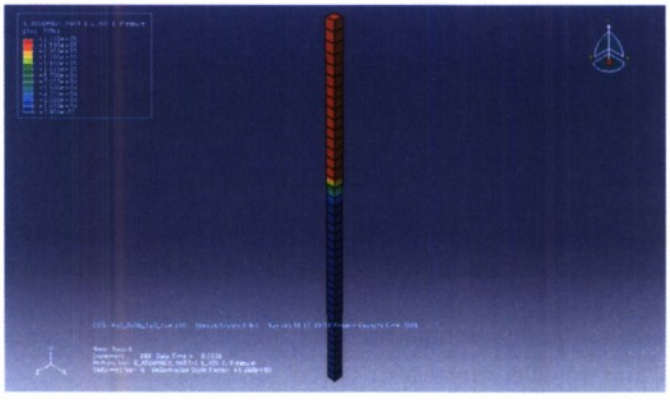

Fig. 14 Air pressure values in computational grid

Symmetry conditions were imposed on the side surfaces as to approximate an infinite air domain. Symmetry conditions were also imposed at the bottom surface of the numerical domain in order to simulate a rigid non-moving surface with perfect reflection. Two loading scenarios were examined. The first shock wave magnitude was set to 0.17 MPa, analogous to the experimental loading observed during the shock tube experiments and the second loading was of magnitude 1.00 MPa (approximately six times the magnitude of the experimental loading).

The data from Table 5 suggests that the numerical values for the shock–particle velocity and the density jump across the shock are reasonably consistent with the respective theoretical values for both the loading scenarios. Theoretical values are derived from shock jump equations (Eqs. 1-3).

Shock Velocity:

$$U_s = a_1 M_1 = \sqrt{\frac{p_1}{\rho_1}}\sqrt{\frac{\gamma+1}{2}\frac{p_s}{p_1}+\gamma} \qquad \textbf{Eq. 1}$$

Particle Velocity:

$$u_s = -u_2 = \frac{p_s}{p_1}\sqrt{\frac{p_1}{\rho_1}}\sqrt{\frac{1}{\frac{\gamma+1}{2}\frac{p_s}{p_1}+\gamma}} \qquad \textbf{Eq. 2}$$

Density ratio:

$$\frac{\rho_2}{\rho_1} = \frac{2\gamma + (\gamma+1)p_s / p_1}{2\gamma + (\gamma-1)p_s / p_1} \quad \textbf{Eq. 3}$$

Table 5. Numerical and theoretical values of shock wave propagation parameters for incoming wave

Loading	0.17 MPa			1.00 MPa		
	Theoretical	Numerical	% Error	Theoretical	Numerical	% Error
Shock Velocity, U_s [m/s]	537.82	531.72	-1.13	1055.7	1102.29	4.41
Particle Velocity, u_p [m/s]	265.62	267.9	0.85	786.75	840.5	6.81
Density Ratio, ρ_2/ρ_1	1.98	1.99	0.51	3.93	4.00	1.78

Material Modeling

The linear Hugoniot shock model in combination with the Mie Grüneisen Equation of State (EOS) are used to model the foam, and the filler materials.

The linear Hugoniot shock model is an empirical relation between shock velocity U_s [m/s] and particle velocity U_p [m/s]:

$$U_s = C_o + sU_p \quad \textbf{Eq. 4}$$

where C_o [m/s] and s are constants determined through experiments.

C_o for many materials has a similar value to the bulk sound velocity C_b (Drumheller, 1998). The bulk sound velocity is a property that can be computed through the experimentally obtained stress–strain curves by the following formula:

$$C_b = \sqrt{\frac{K}{\rho_o}} \quad \textbf{Eq. 5}$$

In order to obtain stress-strain curves for the foam, uniaxial and hydrostatic compression tests were conducted in the Materials and Soils Lab at MIT respectively. Young's modulus, E, for the foam was found to be 1.11 MPa. Bulk modulus, K, was found to be 1.27 MPa. Poisson's ratio, ν was found to be 0.354, which is in typical range of Poisson's ratio values for closed cell foam found in literature (Gibson, 1997).

By substituting the experimentally determined value for the bulk modulus at quasi static loading and the initial density, the bulk sound velocity for the VN 600 foam was found to have a value of **C_b=108.44 m/s**. Value of s in the Eq. 4, for foam was found by interpolation of values of polyurethane foam found in literature (Mader and Carter, 1968). Eventually the linear shock Hugoniot equation for the VN 600 foam takes the form **U_s=108.44 +1.35U_p.**

Equation 6 is the Mie Grüneisen EOS. The Mie Grüneisen EOS is a constitutive model that relates the pressure and internal energy E of a material in reference to the final state of the Hugoniot (p_H,E_H).

$$P = \frac{\rho_o C_b{}^2 \eta}{(1-s\eta)^2} \cdot \left(1 - \frac{\Gamma_o \eta}{2}\right) + \Gamma_o \rho_o e \qquad \textbf{Eq. 6}$$

where p_o: reference density

η=1-p/p_o

Γ_o: Grüneisen parameter

e: internal energy per unit mass

The only parameter that has not been determined in Eqn. 6 is the Grüneisen parameter Γ_o. No information has been found for this parameter which requires a demanding experimental procedure to determine, therefore a value of zero has been used in the simulations. The implication of using a zero value is that the response of the foam plate is considered to be isothermal and no increase of temperature in the foam will be observed.

Table 6 provides the shock Hugoniot parameters and the Grüneisen parameter Γ_o, as obtained from literature (Grady, 1997; Millett, 2005; Kitazawa, 1999; Grover, 1991; Mader, 2009; Marsh, 1980) for some of the filler materials used in this study. Only the C_b value for DERTEX™ foam was experimentally determined in this table.

Table 6. Material properties

Material	ρ_o (kg/m^3)	C_b [m/s]	s	Γ_o
DERTEX^{TM} Foam	108	108.44	1.35	0
Plexiglass	1180	2260	1.82	0.75
Glass Beads	2500	2010	1.8	0
Aerogel	128	567	1.0833	0
Volcanic Tuff	1390	1990	1.22	0
Glycerin	1260	1900	1.8	0.7767
Water	1000	1490	1.92	0.1

Air is modeled using Ideal gas EOS:

$$p + p_a = \rho R(T - T_a) \quad \textbf{Eq. 7}$$

here p_a and T_a are ambient pressure and temperature respectively, R is the gas constant.

Model Description

Geometry and Boundary Conditions

In accordance with the experimental investigation of the problem at hand, two foam configurations were tested; a solid foam specimen and a foam sample with an internal cavity. Glass beads, Aerogel and Volcanic Tuff have been tested in the internal cavity model. The external dimensions of both configurations in the old experiments were 10 in. x 10 in. x 1 in. with a corresponding volume of 100 in^3. An internal core of 8 in. x 10 in. x 0.5 in. was removed from the center of the solid foam specimen in order to model the single cavity configuration. In compliance with the experimental setup, the foam samples were sandwiched between two Plexiglas sheets of 10 in. x 10 in. x 0.125 in. dimension. However, due to the geometric symmetry, only a quarter of the foam samples and Plexiglas sheets were modeled. Therefore, the external dimensions of the combined foam-Plexiglas specimen samples were 5 in. x 5 in. x 1.25 in. while the dimensions of the internal cavity of the quarter plate were 4 in. x 5 in. x 0.5 in. The quarter solid foam sample and single cavity configuration specimen sandwiched between two Plexiglas sheets are depicted in the left and right pictures of Fig. 15 respectively.

The vertical black dashed line (Fig. 15) that is placed on the bottom left edge of the quarter solid domain, corresponds to the center of the whole plate. Additionally, as depicted on the top right corner

of the pictures in Fig. 15, symmetry conditions in the x-axis are imposed on the solid regions inside the green ellipse, while the solid regions inside the red ellipse are bounded by symmetry conditions along the y-axis. During the experiments, the foam samples were constrained on the test stand with the use of 1 in. thick angle beams. It is assumed that the use of these restraining elements is sufficient to hold the sample in place and not allow lateral movement. Therefore, on the regions of the top and bottom surface of the samples, for both solid foam and single cavity configuration, all translational degrees of freedom are constrained in the 1 in. wide regions painted in red in Fig. 16.

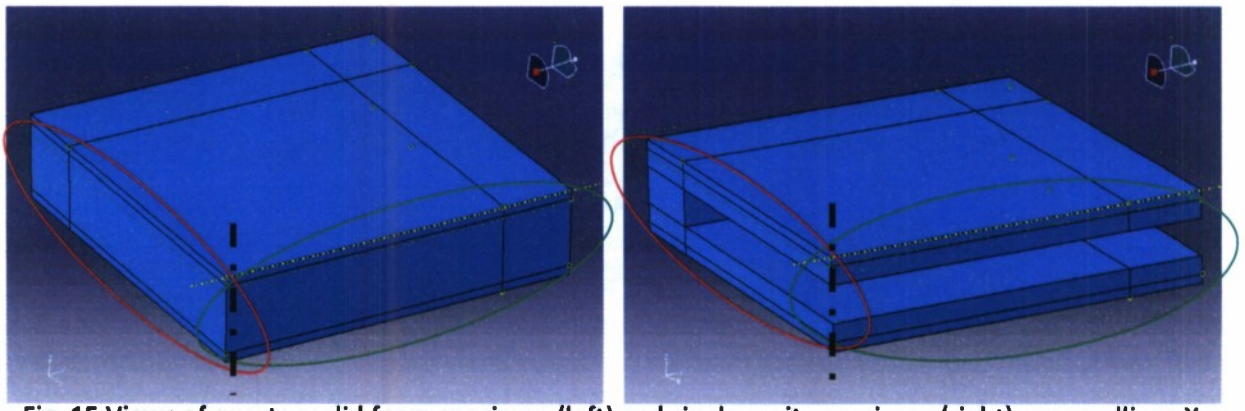

Fig. 15 Views of quarter solid foam specimen (left) and single cavity specimen (right), green ellipse X symmetry, red ellipse Y symmetry

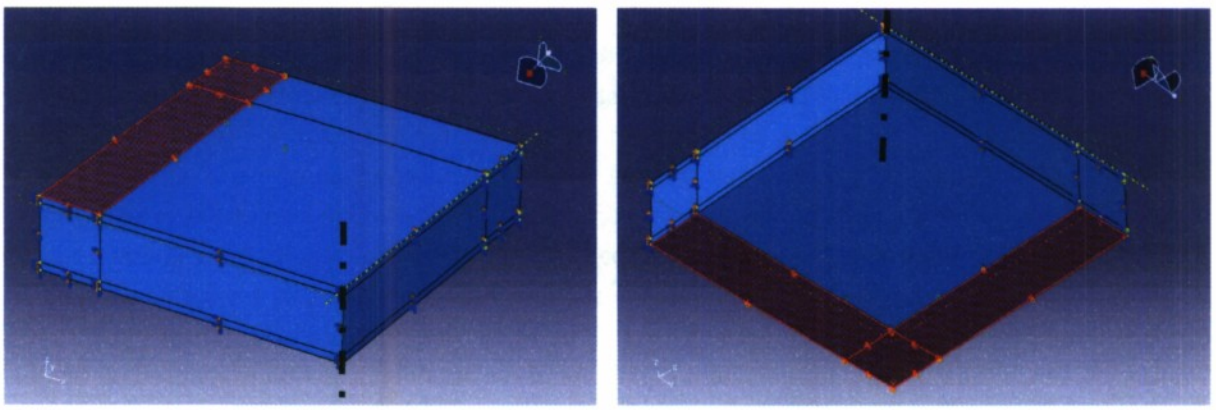

Fig. 16 Regions of constrained translational degrees of freedom on top (left) and bottom surface (right) of solid foam specimen

The Eulerian-fluid domain, depicted in Fig. 17 and 18, employed to model the surrounding air is split in three basic sections A, B and C. The samples are placed initially inside section B of the Eulerian domain with a height of 31.75 mm (1.25 in.).

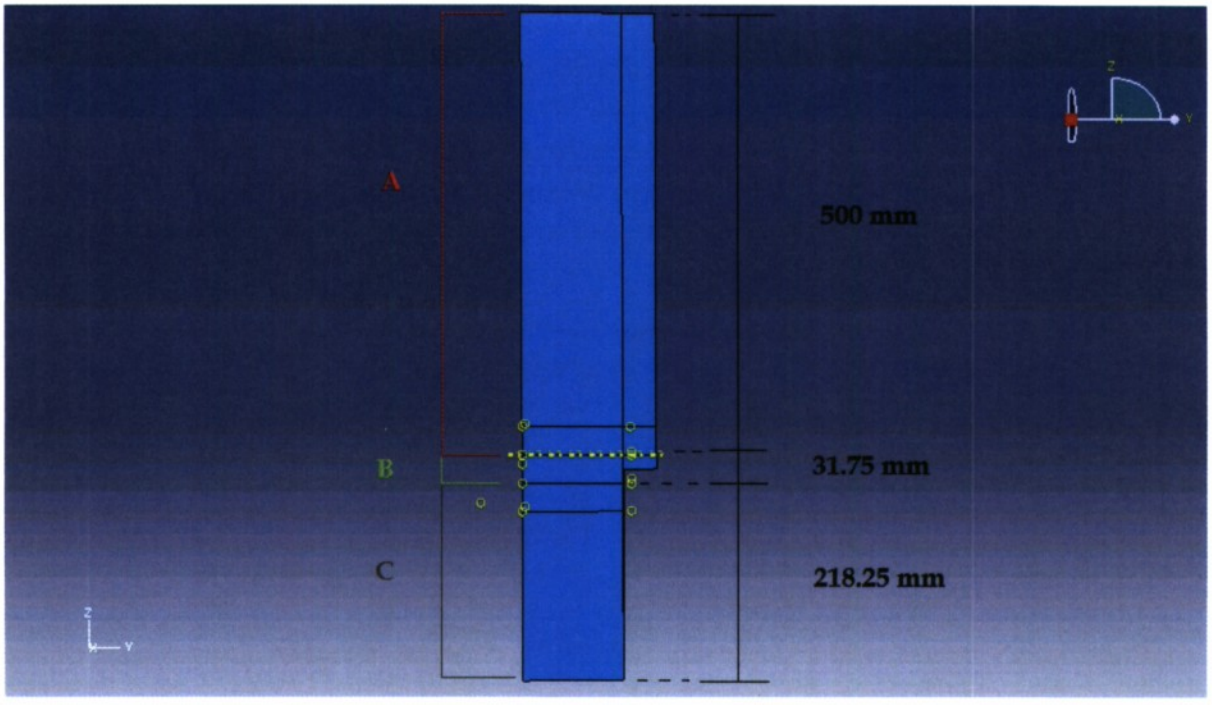

Fig. 17 Eulerian domain

Section A spans 500 mm above the top surface of the solid sample with a cross section of 103.01 mm x 127 mm (4.05 in. x 5 in.). By setting such a distance there is adequate time for the whole incoming shock wave to interact with the samples before any instability affect the measurements. The external loading, simulating the incoming shock wave, is applied on the top surface of section A. The cross section of section A of the Eulerian domain is smaller than the respective cross section of the foam specimens (5 in. x 5 in.). Hence, the long edge of the fluid domain spans along the whole side of the solid (in the y-axis), while the short edge (4.05 in.) in the x-axis spans for only 0.05 inches inside the 1 in. foam region where the translational degrees of freedom are constrained, Fig. . The reasoning behind not expanding the fluid domain also in the x direction, so as to span the whole side of the solid sample similarly to the approach taken in the y direction, stems from the nature of the boundary conditions imposed on the top and bottom 1 in. bands of that solid region. By constraining the translational degrees of freedom on the top and bottom 1 in. regions, the foam material in between would not be able to move. However, this is not the case in the y direction where the boundary conditions are applied only on the bottom surface. The overlap of 0.05 in. between fluid and solid domains is necessary for the fluid-structure interaction extrapolation scheme used in the numerical model.

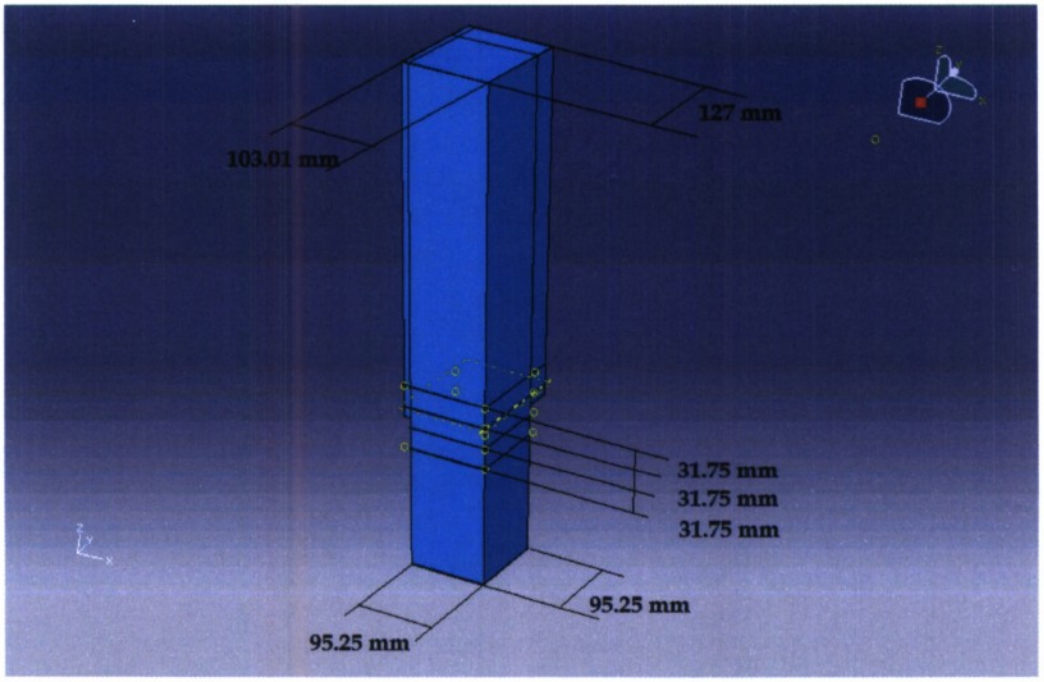

Fig. 18 Isometric view of Eulerian domain

Section C of the air domain has a square cross section with an edge of 95.25 mm (3.75 in.). This section simulates the Plexiglas chamber present behind the sandwiched foam samples during the experimental investigation.

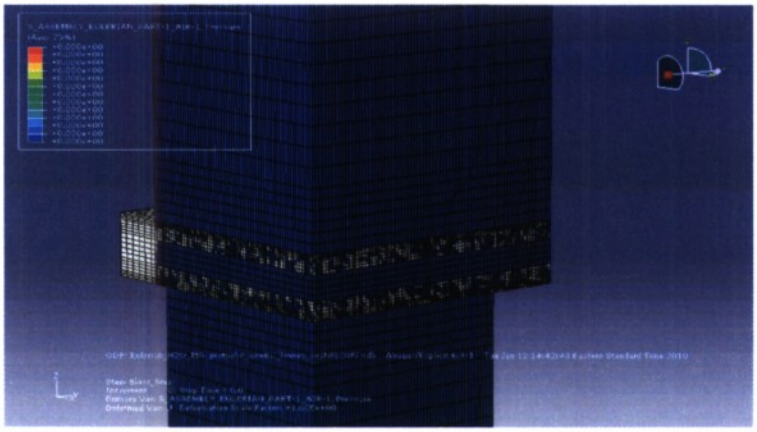

Fig. 19 View of cavity configuration inside Eulerian domain

Due to the geometric symmetry of the problem, only a quarter of the air on top and below the solid specimens has been modeled. The dashed black line in the left picture of Fig. 20 represents the center axis of the full air domain. Accordingly, symmetry boundary conditions have been imposed on the two internal sides of the domain along the center axis. Similarly to the solid domain, symmetry in the x-axis

has been imposed on the side engulfed by the green ellipse of the left picture of Fig. 20, while symmetry in the y-axis on the surface engulfed by the red ellipse. In regards to the external surfaces of the domain (not bound by symmetry), zero displacement boundary conditions in the x-axis and y-axis have been imposed on the surfaces engulfed by the green and red dashed ellipsis respectively of the right picture of Fig. 20. The reasoning behind imposing zero displacement boundary conditions stems from the fact that the top section of the air domain (Section A) should correspond to an infinite air region on top of the plate. Therefore, the displacement of the air elements should be continuous in the direction perpendicular to the shock wave propagation. In the case of Section C of the air domain, the application of such boundary conditions is a result of the presence of the Plexiglas chamber behind the specimens.

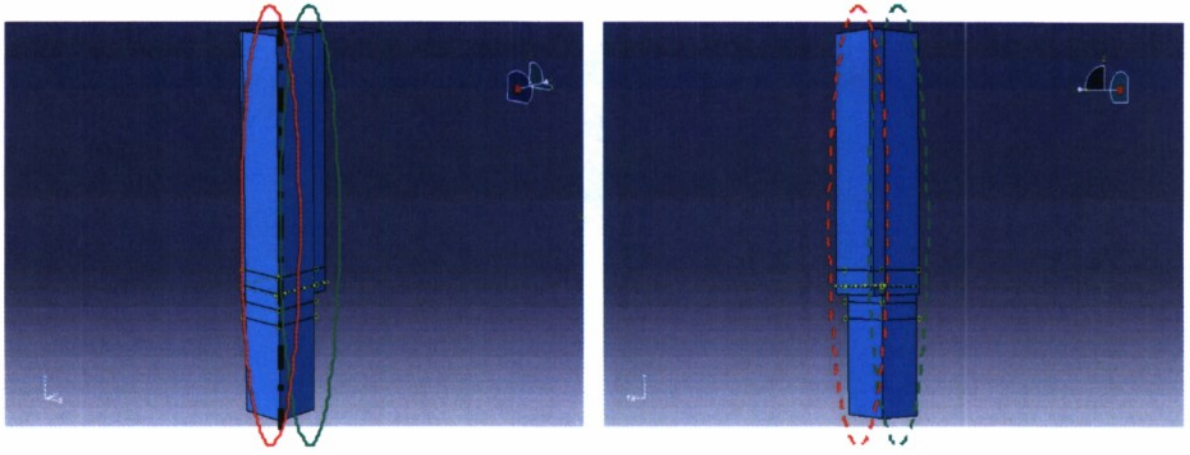

Fig. 20 Boundary conditions imposed on internal (left) and external surfaces (right) of Eulerian domain, solid green ellipse X symmetry, solid red ellipse Y symmetry, dashed green ellipse zero X displacement, dashed red ellipse zero Y displacement.

Mesh and Material Assignment

The Plexiglas and foam regions of both the solid foam and single cavity configuration models were modeled using linear 3D solid continuum elements with enhanced hourglass control. Approximately 13,000 were used to discretize the Plexiglas and foam regions of both solid foam and single cavity configurations. The mesh of the Plexiglas and foam regions of the cavity configuration sample is shown in Fig 21.

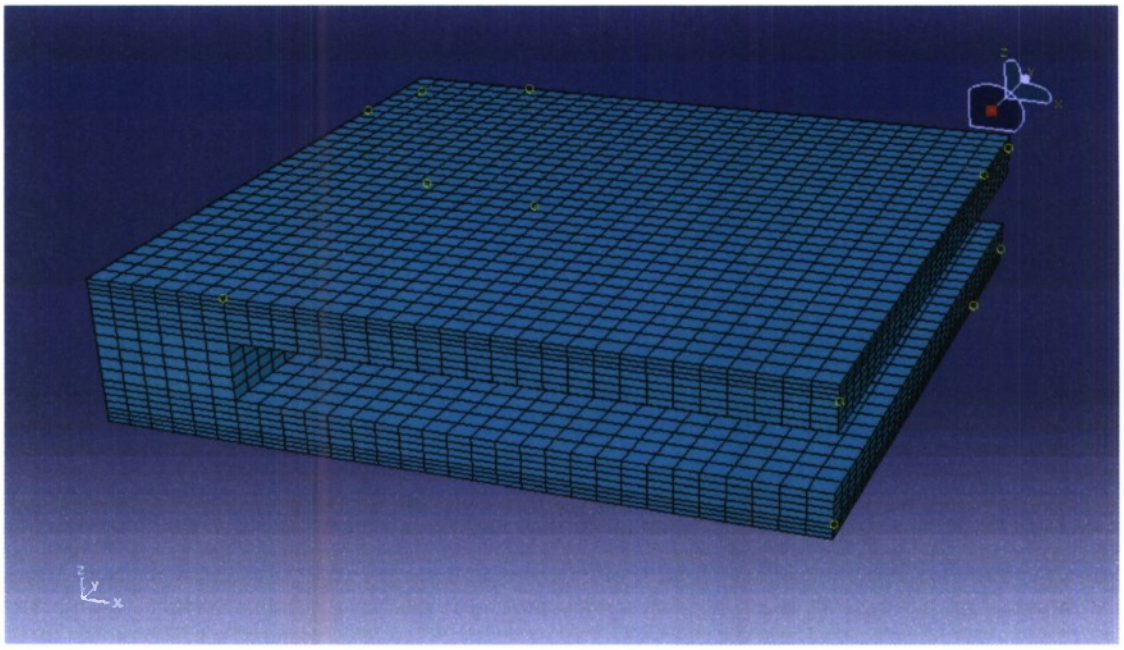

Fig. 21 Single cavity configuration sample mesh

The Eulerian domain is discretized using linear Eulerian 3D elements of the ABAQUS™ element library. A total number of approximately 350,000 were used to model the Eulerian domain, section of which is depicted in Fig 22.

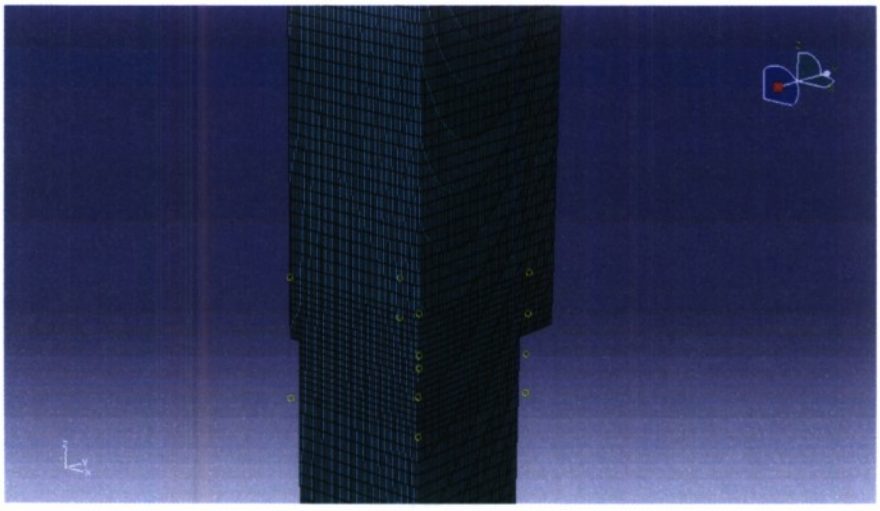

Fig. 22 Eulerian domain mesh

In compliance with the experimental investigation, DERTEX^{TM} VN 600 foam was used to model the foam regions of the examined samples. The foam was modeled using the Hugoniot shock model in combination with the Mie-Grüneisen EOS. Solid filler materials, like Aerogel, Glass Beads and Volcanic Tuff, inside the cavity region were also modeled using the Hugoniot/Mie-Grüneisen EOS, while the surrounding air was described using the EOS for ideal gas.

Loading Conditions

The incoming shock wave is modeled by applying a decaying pressure profile on the top surface of the Eulerian domain, Fig 23, which propagates through section A of the Eulerian domain reaching the top surface of the sample. However, the exact experimentally measured loading profile could not be directly applied on the top surface of the Eulerian domain because of magnitude decay and temporal distribution it experiences while propagating through the top air region.

In order to create loading conditions similar to the experimentally measured profiles, the loading pressure profile on the loading surface was modified in such a way so as to produce a shock of the same magnitude and similar form to the experimental conditions at the distance where the sample is placed. Fig 24 contains the experimentally measured incoming pressure profile, the applied pressure profile on the top of the fluid domain during the numerical simulations and the profile of the incoming wave at a distance of 500 mm from the loading surface. Comparison between the experimentally and numerically experienced incoming shock reveal that the peak overpressure is similar in both cases 24.82 psi (171 KPa), as is the negative phase. On the other hand, the pressure gradient is slightly steeper for the experimental curve. Overall, both curves are similar enough to ensure an appropriate comparison between numerical and experimental loading.

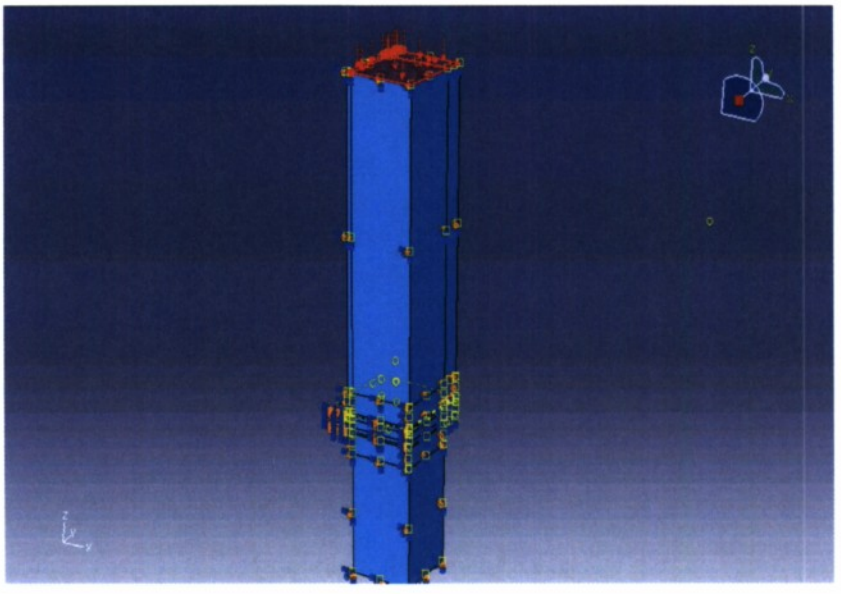

Fig. 23 Surface of Eulerian domain where loading is applied

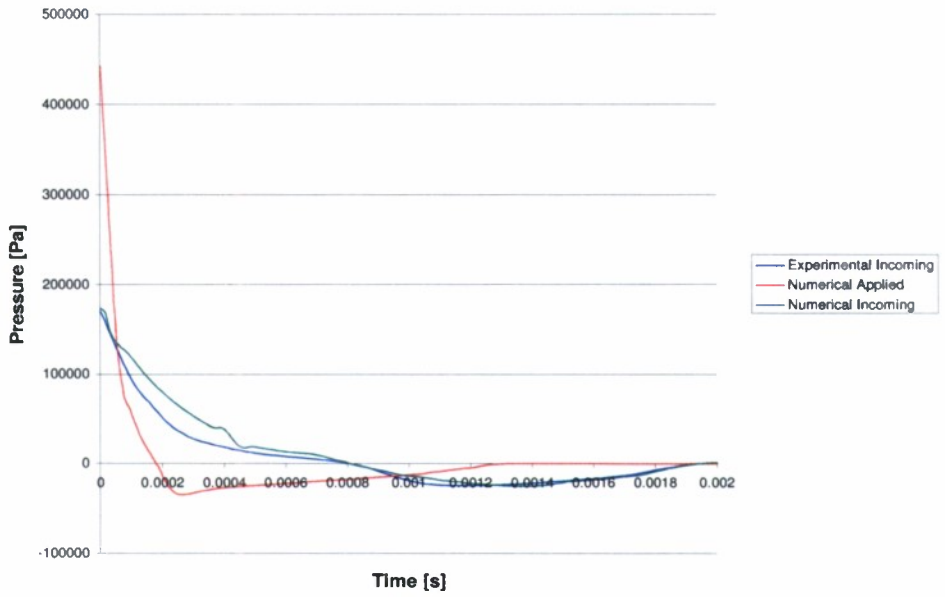

Fig. 24 Experimental and numerical shock wave profiles

Results and Discussion

The simulation parameters mentioned in the previous paragraph are employed during the investigation of the shock response of two sample configurations; a solid foam sample that acts as the control specimen and a single cavity specimen filled with either Aerogel, Glass beads or Volcanic Tuff. The transmitted wave was measured at a distance of 2.75 in. (69.8 mm) from the center of the back surface of the Plexiglass, during the experiments.

Figs. 25-28 shows comparison of pressure profiles obtained experimentally and numerically for solid foam, Aerogel, Glass beads, and Volcanic Tuff. It should be noted that what corresponds to T=0 in these figures is the time at which pressure start rising at point of interest, also referred as point A and which is 2.75 in. behind the sample. As previously mentioned, even though fluid is freely allowed to move through the Eulerian domain, in practice, once the wave reaches the bottom boundary of the domain, numerical disturbances propagate back inside the domain. A close inspection of the transmitted wave propagation shows that these disturbances bounce off the bottom Eulerian boundary and after reaching the measurement location influence the pressure profile. This interference does not affect the numerically derived pressure profile until after approximately 1.0 ms. Hence, all the plots of numerical simulation are cut off after 1 ms. Table 7 shows the comparison of results from experimental and numerical studies.

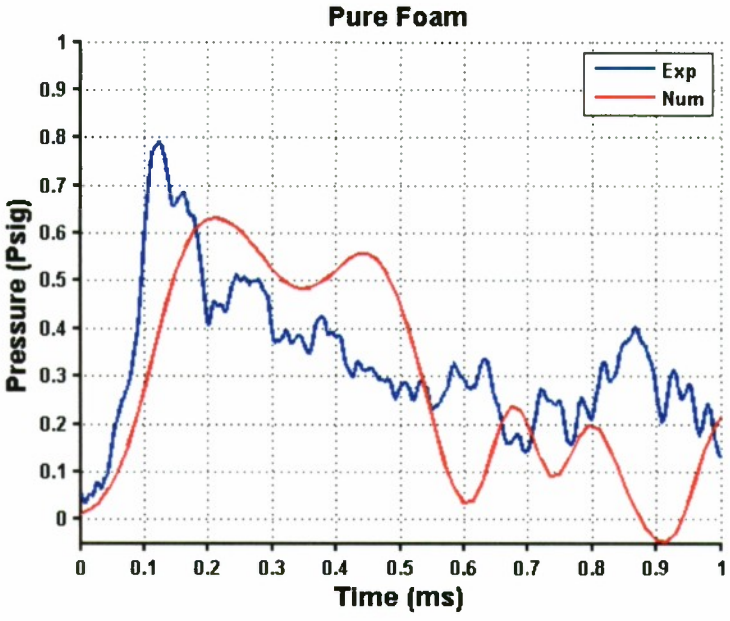

Fig. 25 Comparison of Experimental and Numerical pressures for solid foam

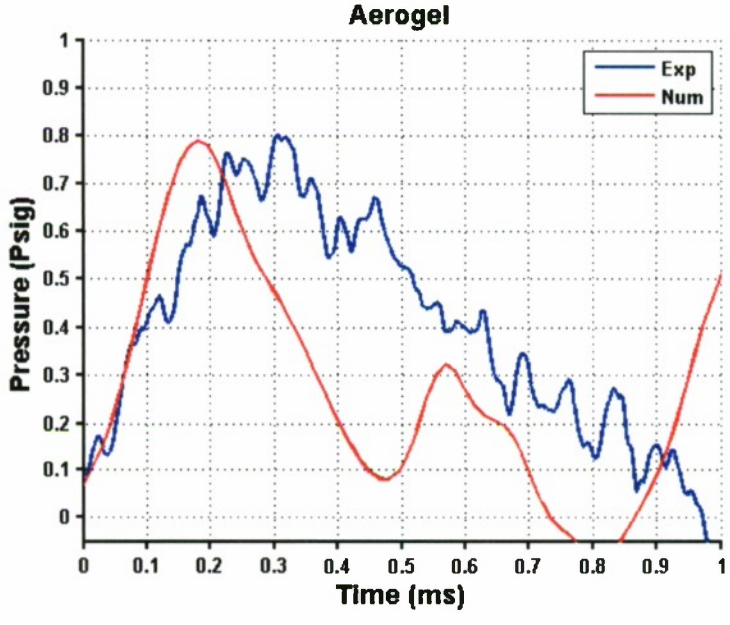

Fig. 26 Comparison of Experimental and Numerical pressures for Aerogel

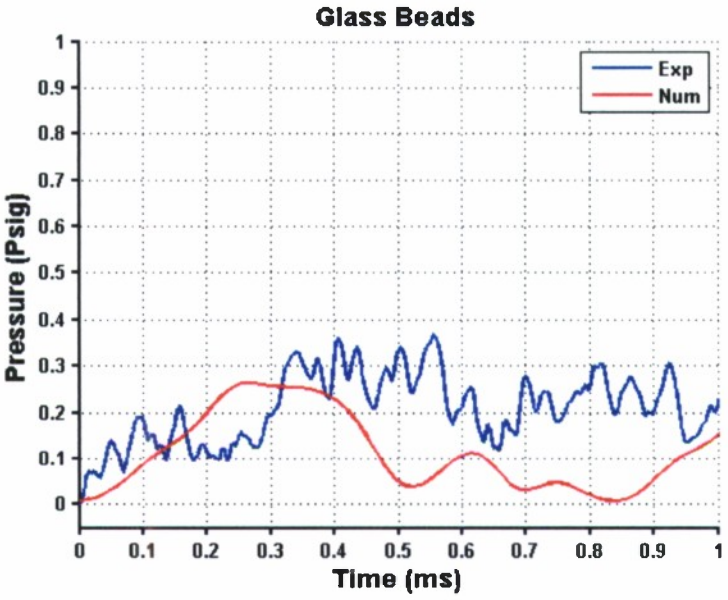

Fig. 27 Comparison of Experimental and Numerical pressures for Glass Beads

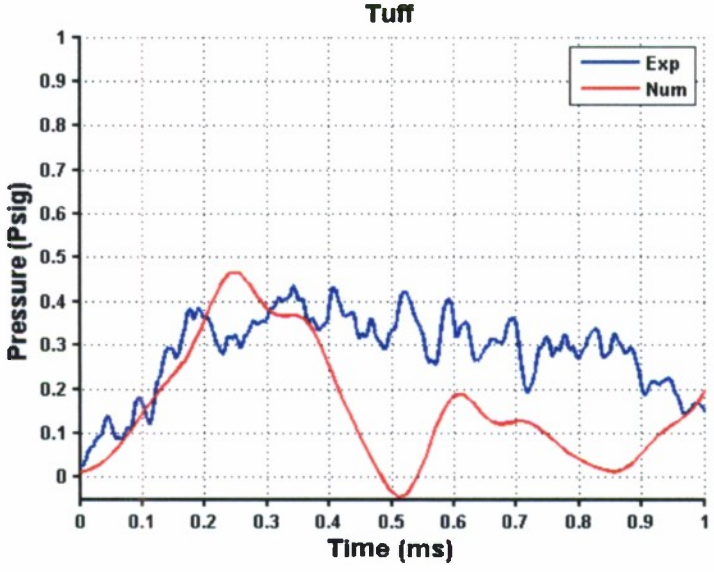

Fig. 28 Comparison of Experimental and Numerical pressures for Volcanic Tuff

Table 7. Comparison of experimental and numerical results

Material	Expt/ Num	Peak Pressure (Psig)	Percentage Change (%)	Rise Time (ms)	Duration (ms)
Solid Foam	E	**0.79**	n/a	0.12	1.27
Solid Foam	N	**0.63**	-20.25	0.20	0.87
Aerogel	E	**0.81**	+2.5	0.30	0.94
Aerogel	N	**0.78**	+23.8	0.18	0.73
Glass Beads	E	**0.36**	-54.43	0.43	1.68
Glass Beads	N	**0.26**	-58.73	0.25	0.84
Tuff	E	**0.43**	-45.56	0.34	1.20
Tuff	N	**0.46**	-26.98	0.24	0.48

As is evident from Figs. 25-28 and Table 7, the numerical results show a partial agreement with the experiments. Peak pressures for filler materials, Aerogel and Volcanic Tuff shows reasonable agreement. But peak pressures for solid foam and Glass beads are off by nearly 20% and 30% respectively. Rise time and time duration do not show good agreement between experiments and numerical. The experimental results shown in Figs. 25-28 are single shot results. Repeatability of these small scale experiments is an issue. Blast propagation is complex and non-linear phenomenon. On repeating these experiments, one can expect to get the peak pressures in the same general range, but not necessarily the overall blast profile as depicted by blue curves in Figs. 25-28.

Shock wave propagation using coupled Eulerian-Lagrangian technique is tried for the first time using ABAQUS™, so there is no documented literature available to assist in modeling issues. We have addressed the numerical issues we have come across with the technical support of ABAQUS™, and we hope to get reasonable agreement between simulations and the experiments in few weeks.

The analyses of the transmitted wave focused on following the pressure profile at a specific location for the duration of the simulation. The following surface plot (Fig. 29) depicts the pressure values at the

integration point of all the elements at point A for one time instant. The objective of surface plots like this is to provide insight into the spatial distribution of the transmitted pressure values at a specific distance from the tested samples. The scale on the right of Fig. 29 is in Pascals.

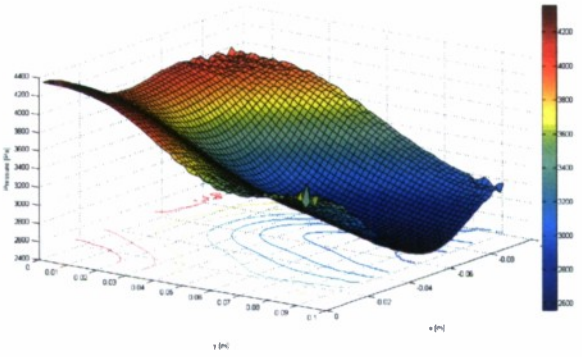

Fig. 29 Spatial distribution of pressure, at the moment when point A attains peak pressure for solid foam case

Conclusions

To summarize the results from numerical analysis. So far we have been able to successfully validate the propagation of shock wave through air using ABAQUS™. And there is partial agreement between the numerical results and the experiments. Peak pressures are in the same ball park, but rise times and durations are not. We have identified the potential reasons for this discrepancy and hope to overcome these in few weeks. Once the numerical model is validated, the idea is to use the model to assist in design of experiments. Various parametric studies can be conducted across a range of geometries and material properties, to find an optimum combination. Many parameters for example, spatial distribution of pressure, which can't be obtained experimentally can be obtained numerically, and can give insight about the spatial distribution.

We have also started modeling 3D helmet liner. This model coupled with the human head model (Fig. 30) from Prof. Raul Radovitzsky's group (Soldier Nanotechnology Lab, MIT), can provide important insight as how the blast wave after passing through the helmet liner affects the brain tissues.

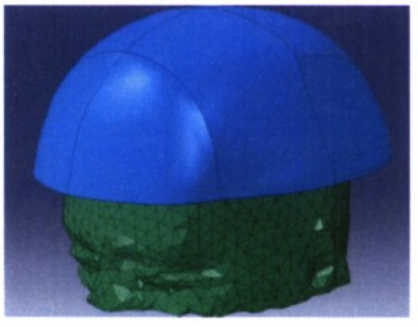

Fig. 30 Integrated 3D liner model with human head model

Exploitation of Research Results

Poster

Alley, M., Son, S.F., Christou, G., Goel, R., and Young, L.R., "Experimental Studies of Mitigation Materials for Blast Induced TBI", 16th APS Tropical Conference on Shock Compression of Condensed Matter, Nashville, TN, 28 June - 3 July, 2009.

Presentations

Young, L., Son, S., Christou, G., Goel, R., Alley, M., "A Fluid Helmet Liner For Protection Against Blast Induced Trauma", ONR CIED BR Program Review, Johns Hopkins University, 4-7 Nov, 2008.

Son, S., Young, L., Christou, G., Goel, R., and Alley, M., "Blast Mitigation for Protection against Blast Induced Trauma", DHS Blast Mitigation Workshop, 30 April 2009, Kingston, RI.

Young, L., Son, S., Christou, G., Goel, R., Alley, M., "A Fluid Helmet Liner For Protection Against Blast Induced Trauma", ONR CIED BR Program Review, University of Washington, 26-29 Oct, 2009.

Goel, R., Vechart, A., Christou, G., and Young, L.R., "Development of a Helmet Liner for Protection against Blast Induced Trauma", IMPLAST 2010, SEM Fall Conference, Providence, RI, USA, 12-14 Oct, 2010.

Theses

Alley, M., "Explosive Blast Loading Experiments For TBI Scenarios: Characterization and Mitigation", Master's Thesis, Purdue University, Aug 2009.

Christou, G., "Development of a Helmet Liner for Protection Against Blast Induced Trauma", Master's Thesis, MIT, Feb 2010.

List of Figures

List of Tables

References

1. Allen, R. M., Kirkpatrick, D. J., Longbottom, A. W., Milne, A. M., and Bourne, N. K., "Experimental and numerical study of free-field blast mitigation, " *Shock Compression of Condensed Matter*, 2003, Portland, OR.

2. Calogne, R., and Fluidos, S. L., "Resistant Helmet Assembly", US Patent 5815846, 1998.

3. Drumheller, D. S., *Introduction to Wave Propagation in Nonlinear Fluids and Solids*, Ca bridge University Press, United Kingdom, 1998.

4. Kinney, G. F. and Graham, K. K., *Explosive Shocks in Air*, 2nd Ed., Springer-Verlag New York Inc., New York, 1985.

5. Li, Q. M., and Meng, H., "Attenuation or enhancement - a one-dimensional analysis on shock transmission in the solid phase of a cellular material," *International Journal of Impact Engineering*, Vol. 27, 2002, pp. 1049-1065.

6. Gerber, F., et al., "Armor and a method of manufacturing it", US Patent 4665794, 1987.

7. Gibson, L., Ashby, M. F., *Cellular Solids Structure and Properties*, Cambridge University Press, 1997, Cambridge.

8. Gooding, E. R., "Energy-Absorbing Insert for Protective Headgear", US Patent 4375108, 1983.

9. Grady, D. E., and Chhabildas, L. C., "Shock-wave properties of soda-Lime glass", *Proceedings for the 4th US Army Symposium on Solid Mechanics*, Myrtle Beach, South Carolina, Battelle Press, Columbus, pp. 29–38, 1997.

10. Grover ,R., Ree, F. A., and Holmes, N., "Equation of state from SiO2 Aerogel Hugoniot data", *1991 APS Topical Conference on Shock Compression and Condensed Matter*, Williamsburg, VA, June 17-20, 1991.

11. Groves, T. K., and Groves, D., "Body Armor", US Patent 5087516, 1992.

12. Holt, M. C., and Tomczak, W. F., "Protective Gear with Hydraulic Liner", US Patent 3849801, 1974.

13. Homae, T., Wakabayashi, K., Matsumura, T., and Nakayama, Y., "Reduction of explosion damage using sand or water layer", *Shock Compression of Condensed Matter, 2007, Waikoloa, HI.*

14. Hosaka, "Helmet and Fluid Reservoir System", US Patent 5148950, 1992.

15. Kitazawa, Y., Fujiwara, A., Kadono, T., Imagawa, K., Okada, Y., and Uematsu, K., "Hypervelocity impact experiments on aerogel dust collector", *Journal of Geophysical Research*, Vol. 104, No. E9, pp. 22035-22052, 1999.

16. Mader, C., and Carter, W., An equation of State for Shocked Polyurethane Foam, Los Alamos Scientific Laboratory, New Mexico, 1968.

17. Mader, C. L., "Numerical Modeling of Crater Formation by Meteorite Impact and Nuclear Explosion", *In Predictive Modeling of Dynomic Processes*, Springer, 2009, Part 3, pp. 447-457

18. Marsh, S. P., "LASL Shock Hugoniot Data", University of California Press, Berkeley, 1980.

19. Mendoza, I. D., "Safety Helmet", US Patent 6560787, 2003.

20. Millett, J. C. F., Bourne, N. K., Akhavan, J., and Milne, A. M., "The response of soda-lime glass-hydroxyterminated polybutadiene composites to shock loading", *Journol of Applied Physics*, Vol. 97, 043524 (2005).

21. Morgan, G. E., "Energy Absorbing and Sizing Means for Helmets", US Patent 3609764, 1971.

22. Nesterenko, V. F., "Shock (blast) mitigation by "soft" condensed matter", *2003 MRS Foll Meeting, 2003, Boston, MA.*

23. Ponomarev, V., and Ponomaryova, I., "Blast Compression Wave Absorbing Device", US Patent 7017705, 2006.

24. Rhoades, L. J., Matechen, J. M., and Rosner, M. J., "Smart Padding System Utilizing an Energy Absorbent Medium and Articles made there from", US Patent 6701529, 2004.

25. Stewart D., A Protective Helmet Liner Incorporating Fluid Channels, MS Thesis, UCD School of Electrical, Electronic and Mechanical Engineering, Dublin, 2008.

26. Stuhmiller, J. H., Chan, P., and Stuhmiller, L., "Anti-Blast and Shock Optimal Reduction Buffer", US Patent 250548, 2008.

27. Villari, F. K., Steigerwald, C. J., and Rappleyea, F. A., "Protective Helmet", US Patent 3994021, 1976.

28. Zhuang, S., Ravichandran, G., and Grady, D. E., "An experimental investigation of shock wavepropagation in periodically layered composites," *Journal of the Mechonics ond Physics of Solids*, Vol. 51, 2003, pp. 245-265.

Development of a Helmet Liner for Protection Against Blast Induced Trauma

by

George Alexander Christou

Submitted to the Department of Aeronautics and Astronautics

on January 29, 2010, in partial fulfillment of the

requirements for the Degree of Master of Science in

Aeronautics and Astronautics

Abstract

Traumatic brain injuries caused by shock waves have attracted increased medical and scientific attention due to the large percentage of combat troops that have sustained such injuries in recent conflict theatres. To this day, the knowledge in the fields of causes, effects and identification of traumatic brain injury is limited. The use of advanced body armor has decreased the number of fatalities from fragments observed in previous military operations, resulting in the increase of non-fatal brain injuries from shock waves.

The purpose of this project is the advancement of the knowledge in the field of shock wave mitigation strategies and the development of a helmet liner for protection against blast induced trauma. The proposed helmet liner design is based on the introduction of solid and fluid filler materials inside channels opened in the interior of a foam liner in order to enhance the attenuation of incoming shock waves. Primary investigated attenuation mechanisms include acoustic impedance mismatches between the filler and foam material interfaces, viscous effects of fluid fillers, porosity and particle size of solid filler materials. Specific goals of this research project include the reduction of the peak pressure and pressure gradient of the transmitted wave through the helmet liner and the enhancement of the spatial distribution of the energy of the incoming shock wave.

This research effort employed both shock tube experiments and numerical studies in order to investigate the effectiveness of the proposed helmet liner design. Quantitative results have shown that the use of high density filler materials result in higher attenuation levels than low density materials while comparing to solid foam

control samples. The peak transmitted overpressure and pressure gradient were significantly reduced with the use of high density materials while the duration of the positive phase was increased. This response resulted in lower overall impulse values of the transmitted wave. The use of high density filler materials also results in superior frequency distribution.

Thesis Supervisor: Laurence R. Young
Apollo Program Professor of Astronautics
Professor of Health Sciences and Technology

ABSTRACT

Alley, Matthew David. M.S.M.E., Purdue University, August, 2009.
Explosive Blast Loading Experiments for TBI Scenarios: Characterization and Mitigation. Major Professor: Dr. Steven F. Son. School of Mechanical Engineering.

As a result of the growing military conflicts over the past eight years, the focus on traumatic brain injuries sustained from explosive blasts in wartime scenarios has gained tremendous attention in the scientific and medical communities. During previous warfare conflicts in history, military armor was not as technologically advanced as it is today. As a result, the understanding of traumatic brain injuries is limited since previous blast occurrences typically resulted in higher fatalities due to non-primary blast effects. It is, therefore, the intent of this work to advance the knowledge on traumatic brain injuries from explosive blasts. The study focuses on two aspects. The first focus is on surrogate modeling of the human anatomy subjected to blast loading conditions and the resulting behavior that occurs which provides insight into injury mechanisms and needed model validation data. The second focus is on preventive protection against explosive blasts by studying various materials and the effectiveness of each material to attenuate blast profile characteristics.

The physical modeling aspect of the study was accomplished by varying surrogate materials, geometric configuration, and blast loading conditions in order to determine the measurable behavior variations. Quantitative results were obtained through pressure, acceleration, strain, and displacement measurements. These results suggested large initial amplification of pressures

at anterior locations near the shell/gel interface. Material property effects and geometric features effects were seen by larger responses with the material of lower stiffness and more severe responses with the facial feature shell models over the solid shell models. Extreme accelerations were experienced with oscillatory behavior over the duration of the blast. In addition, significant relative displacement was observed between the shell and the gel material suggesting large strain values. Further quantitative results were obtained through shadowgraph imaging of the blast scenarios. The shadowgraph imaging confirmed the approximation that global movement of the target was minimal during the blast occurred on a different time scale. The complete results then provided a means of comparison to actual measured behavior from surrogate models to injury mechanisms in computational and clinical trials. Furthermore, the data obtained can be used in computational validation.

The blast mitigation aspect of the study was accomplished by applying blast loading conditions to various mitigant materials. Composite structures were constructed using various filler materials which varied density, porosity, viscosity, and particle size. Quantitative results were then obtained by measuring transmitted wave profiles behind the respective samples and comparing to free-field loading conditions. Attenuation effectiveness was then determined by the reduction of blast profile characteristics (peak overpressure, pulse duration, and impulse). The results of these experiments showed that lower density, porous materials caused blast profile resembling scaled air blasts. Specifically shorter wave front rise times and negative overpressure values were observed. The higher density materials exhibited the greatest attenuation by lower the overall peak pressure, lengthening the duration, and slowing the rise to peak amplitude. This resulted in lower overall impulse values. Furthermore, significant frequency distribution was observed surpassing the effectiveness of the solid foam control sample and the lower density materials.